J Comput Neurosci (2012) 33:495–514
DOI 10.1007/s10827-012-0397-5

Calcium control of triphasic hippocampal STDP

Daniel Bush · Yaochu Jin

Received: 14 October 2011 / Revised: 7 April 2012 / Accepted: 11 April 2012 / Published online: 19 May 2012

Abstract Synaptic plasticity is believed to represent the neural correlate of mammalian learning and memory function. It has been demonstrated that changes in synaptic conductance can be induced by approximately synchronous pairings of pre- and post- synaptic action potentials delivered at low frequencies. It has also been established that NMDAr-dependent calcium influx into dendritic spines represents a critical signal for plasticity induction, and can account for this spike-timing dependent plasticity (STDP) as well as experimental data obtained using other stimulation protocols. However, subsequent empirical studies have delineated a more complex relationship between spike-timing, firing rate, stimulus duration and post-synaptic bursting in dictating changes in the conductance of hippocampal excitatory synapses. Here, we present a detailed biophysical model of single dendritic spines on a CA1 pyramidal neuron, describe the NMDAr-dependent calcium influx generated by different stimulation protocols, and construct a parsimonious model of calcium driven kinase and phosphatase dynamics that dictate the probability of stochastic transitions between binary synaptic weight states in a Markov model. We subsequently demonstrate that this approach can account for a range of empirical observations regarding the dynamics of synaptic plasticity induced by different stimulation protocols, under regimes of pharmacological blockade and metaplasticity. Finally, we highlight the strengths and weaknesses of this parsimonious, unified computational synaptic plasticity model, discuss differences between the properties of cortical and hippocampal plasticity highlighted by the experimental literature, and the manner in which further empirical and theoretical research might elucidate the cellular basis of mammalian learning and memory function.

Keywords Synaptic plasticity · Calcium · Learning · Memory · Hippocampus

Action Editor: Carson C. Chow

Electronic supplementary material The online version of this article (doi:10.1007/s10827-012-0397-5) contains supplementary material, which is available to authorized users.

D. Bush
UCL Institute of Cognitive Neuroscience,
London WC1N 3AR, UK

D. Bush (✉)
UCL Institute of Neurology,
London WC1N 3BG, UK
e-mail: drdanielbush@gmail.com

Y. Jin
Department of Computing, University of Surrey,
Guildford GU2 7XH, UK

1 Introduction

Synaptic plasticity—the process of activity dependent change in synaptic conductance—is widely believed to represent the neural correlate of mammalian learning and memory function (Hebb 1949; Martin et al. 2000; Whitlock et al. 2006). Since the first experimental demonstrations of long-term potentiation (LTP) and depression (LTD), a wealth of empirical data regarding the induction, expression and maintenance of synaptic plasticity in different cortical regions has been obtained (Lomo and Bliss 1973; Dudek and Bear 1992; Malenka and Nicoll 1999; Citri and Malenka 2008; Neves et al. 2008). In spite of the heterogeneity of plasticity mechanisms observed throughout the brain, changes in the strength of excitatory synapses afferent on CA1 pyramidal neurons in the hippocampus represent the best studied form in the mammalian cortex (Malenka and Bear 2004;

Cooke and Bliss 2006; Bliss et al. 2007; Nelson and Turrigiano 2008). At these synapses, calcium influx into dendritic spines represents a critical signal for synaptic plasticity induction (Lisman 1989; Artola and Singer 1993; Yang et al. 1999; Cormier et al. 2001; Mizuno et al. 2001; Shouval et al. 2002; Sjostrom and Nelson 2002; Buchanan and Mellor 2010). Large, transient elevations in intracellular [Ca^{2+}] generate LTP via the preferential activation of kinase pathways while modest, sustained elevations in intracellular [Ca^{2+}] generate LTD via the preferential activation of phosphatase pathways (Malenka et al. 1989; Malinow et al. 1989; Hanson and Schulman 1992; Mulkey et al. 1993; Lee et al. 2000). Initial empirical observations of synaptic plasticity were mediated by tetanic stimulation protocols, with high frequency stimulation (HFS; typically 1 s of 100 Hz afferent firing) used to induce LTP and low frequency stimulation (LFS; typically 15mins of 1 Hz afferent firing) used to induce LTD (Lomo and Bliss 1973; Dudek and Bear 1992). In more recent years, it has also been established that temporally correlated pairs or triplets of pre- and post- synaptic action potentials delivered at low frequencies can induce bidirectional spike-timing dependent plasticity (STDP) depending, among other parameters, on their exact temporal offset over a range of ~100 ms (Bi and Poo 1998; Debanne et al. 1998; Pike et al. 1999; Wittenberg and Wang 2006; Buchanan and Mellor 2007; Nishiyama et al. 2000; Meredith et al. 2003). STDP has been examined in a variety of cortical regions and species, and its discovery has both accompanied and accelerated a move in computational neuroscience from rate to temporally coded models of cognitive processing (Caporale and Dan 2008; Shouval et al. 2010).

Early studies of STDP, primarily carried out in hippocampal cell cultures, delineated a straightforward relationship between the relative timing of single pre- and post- synaptic action potentials and subsequent changes in synaptic strength (Fig. 1a; (Bi and Poo 1998; Debanne et al. 1998)). However, more recent examinations using acute hippocampal slices have been unable to induce bidirectional plasticity with pairs of single pre- and post- synaptic action potentials under standard recording conditions (Fig. 1b; (Pike et al. 1999; Wittenberg and Wang 2006; Buchanan and Mellor 2007; Nishiyama et al. 2000; Meredith et al. 2003)). These results suggest a more complex picture where synaptic plasticity is dependent not just on relative spike timing, but also on the frequency, duration and nature of spike pairings—with a triphasic STDP curve obtained at CA3-CA1 synapses only when pairings are delivered at approximately theta frequency (>5 Hz) and involve multiple post-synaptic spikes ((Buchanan and Mellor 2010; Pike et al. 1999; Wittenberg and Wang 2006; Shouval et al. 2010); Fig. 1c). Similar results have been acquired at excitatory connections between cortical pyramidal neurons (Sjöström et al. 2001). Other experimental data indicates that potentiation and depression events are switch-like transitions between binary conductance states, mediated by kinase and phosphatase pathways that are competitive and co-activated (Petersen et al. 1998; O'Connor et al. 2005a; O'Connor et al. 2005b; Bagal et al. 2005; Fukunaga et al. 2000). The kinetics of kinase and phosphatase activation also differ significantly, as LTP can be rapidly induced by appropriate activity patterns while LTD requires prolonged stimulation (Yang et al. 1999; Mizuno et al. 2001; Wittenberg and Wang 2006). Furthermore, changes in synaptic conductance decay over a period of hours unless they are accompanied and consolidated by *de novo* protein synthesis (Krug et al. 1984; Nguyen et al. 1994; Frey and Morris 1997).

Early theoretical models of STDP were primarily phenomenological, dictating changes in synaptic weight according to the relative timing of pre- and post- synaptic spiking alone (Song et al. 2000; Froemke et al. 2006; Pfister and Gerstner 2006). These models are computationally tractable, but generally fail to replicate synaptic plasticity data obtained using other stimulation protocols. Subsequent modeling work has demonstrated that intracellular calcium dynamics—primarily dictated by influx through the NMDA receptor (NMDAr), although significant alternative sources do exist (see (Sjöström et al. 2008) for a review)—are sufficient to account for empirical data obtained using multiple stimulation protocols (Shouval et al. 2002; Zhabotinsky 2000; Karmarkar and Buonomano 2002; Abarbanel et al. 2003; Abarbanel et al. 2005; Rubin et al. 2005; Shouval and Kalantzis 2005; Graupner and Brunel 2007; Pi and Lisman 2008; Urakubo et al. 2008; Rackham et al. 2010, for reviews see (Graupner and Brunel 2010; Froemke et al. 2010)). This calcium control hypothesis integrates a wide array of experimental data within a single theoretical framework and naturally generates a triphasic STDP window of the type observed in acute hippocampal slice studies, as intermediate calcium concentrations leading to LTD are generated by both acausal (i.e. post-pre) spike pairings at short temporal offsets and causal (i.e. pre-post) spike pairings at longer temporal offsets. Subsequent studies have attempted to modify the calcium control hypothesis in order to account for the biphasic learning curve observed in hippocampal cultures and at cortical synapses by integrating stochasticity, an explicit veto system that circumvents intermediate calcium concentrations generated by causal spike pairings, or segregating the mechanisms of LTP and LTD induction (Karmarkar and Buonomano 2002; Shouval and Kalantzis 2005; Rubin et al. 2005; Graupner and Brunel 2007; Urakubo et al. 2008). However, very few models have considered the dynamic nature of transitions between binary high and low synaptic conductance states—the majority implementing instantaneous, graded changes in synaptic weight at a uniform rate ((Shouval et al. 2002; Karmarkar and Buonomano 2002; Abarbanel et al. 2003; Shouval and Kalantzis 2005; Rubin et al. 2005;

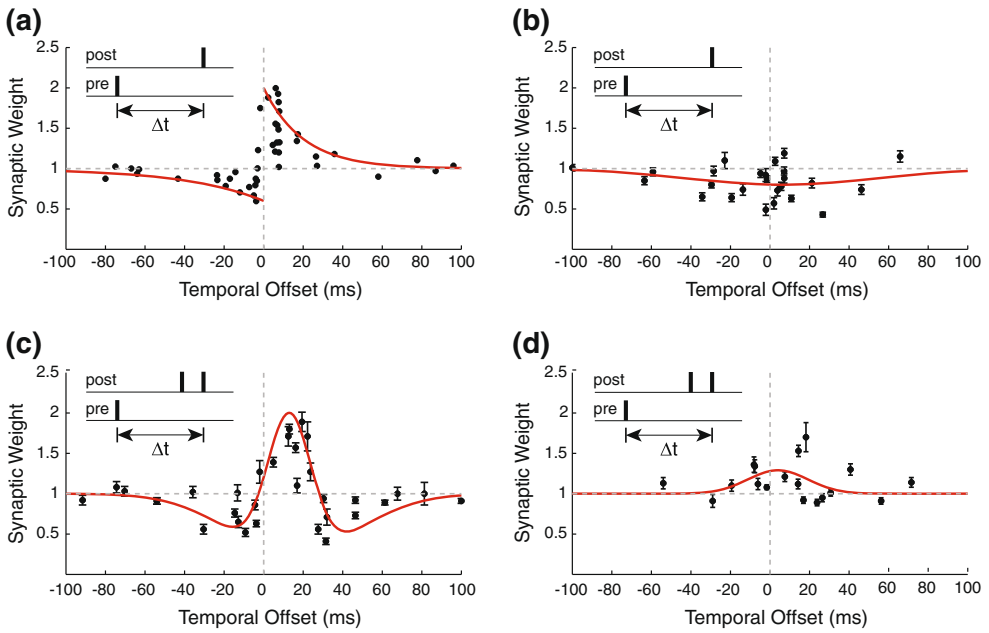

Fig. 1 Summary of the STDP data obtained in hippocampal cell cultures [from Bi and Poo 1998] and acute slice preparations [from Wittenberg and Wang 2006]. **(a)** The change in synaptic weight generated by 100 pairs of single pre- and post- synaptic spikes at 1 Hz and various temporal offsets ($\Delta t = t_{post} - t_{pre}$) in hippocampal cell cultures, and two exponential curves fit to this data (with $A_+ = 1$, $\tau_+ = 20$ ms, $A_- = -0.4$ and $\tau_- = 40$ ms) from (Bi and Poo 1998). **(b)** The change in synaptic weight generated by 100 pairs of single pre- and post- synaptic spikes at frequencies of 0.1 - 5 Hz in acute slice preparations and a Gaussian fit to this data (with $\mu = 6$ ms, $\sigma = 48$ ms and a peak of 0.8) from (Wittenberg and Wang 2006). **(c)** The change in synaptic weight generated by 100 pairings of single pre-synaptic spikes with two post-synaptic spikes at 5 Hz in acute slice preparations and the sum of two Gaussians fit to this data (with $\mu_1 = 15$ ms, $\sigma_1 = 32$ ms and $\mu_2 = 13$ ms, $\sigma_2 = 11$ ms) from (Wittenberg and Wang 2006). **(d)** The change in synaptic weight generated by 30 pairings of single pre-synaptic spikes with two post-synaptic spikes at 5 Hz in acute slice preparations and a Gaussian fit to this data (with $\mu = 4$ ms, $\sigma = 15$ ms and a peak value of 1.29) from (Wittenberg and Wang 2006)

Graupner and Brunel 2007; Rackham et al. 2010), but see (Abarbanel et al. 2005; Pi and Lisman 2008)).

Here we present a new model, based on the calcium control hypothesis, which incorporates several novel features that allow recent experimental data to be more accurately replicated. The model is comprised of binary synapses, with the frequency and relative conductance of high and low weight states matched to empirical recordings, and transitions between these states governed by a Markov model (Petersen et al. 1998; O'Connor et al. 2005a). Transition probabilities are non-zero at rest and dictated by calcium concentration within the dendrite during stimulation such that changes in synaptic strength can take place at any time and generally occur sometime after a stimulus, as observed experimentally (Wittenberg and Wang 2006; O'Connor et al. 2005a; Bagal et al. 2005). We putatively associate these dynamic, calcium driven transition probabilities with kinase and phosphatase activity, and subsequently put them under the control of novel thresholded Hill function inspired by recent advances in systems biology (Morgan 2007; Buchler and Cross 2009). The dynamic probability of low→high and high→low weight transitions, corresponding to potentiation and depression respectively, also obey distinct kinetics, such that LTP is expressed more rapidly, and the ratio of non-zero resting probabilities replicates the experimentally observed decay of early-phase potentiation and depression over a time course of ~1 h (Wittenberg and Wang 2006; O'Connor et al. 2005a; Bagal et al. 2005; Krug et al. 1984; Nguyen et al. 1994; Frey and Morris 1997). We tune the parameters of this model to specifically account for observations of triphasic hippocampal STDP made in acute slice preparations and subsequently demonstrate that it can parsimoniously replicate the dependence of synaptic plasticity on stimulation frequency and duration, as well as the dynamics of synaptic weight change and decay. We utilise this model to infer the time course of residual depolarisation in the spine generated by backpropagating action potentials (bAPs) and the magnitude of NMDAr-dependent calcium influx when significant depolarisation follows glutamate binding by >50 ms; and then show that it can also replicate observations of synaptic plasticity induced by a number of other stimulation protocols, under regimes of selective pharmacological blockade and metaplasticity. Finally, we discuss the general strengths and weaknesses of this parsimonious, unified computational synaptic plasticity model, differences in the properties and mechanisms of cortical and hippocampal plasticity described by the experimental literature, and the manner in which further empirical and theoretical research might elucidate the cellular basis of mammalian learning and memory function.

2 Results

We examine a detailed biophysical model of a single dendritic spine that receives pre- and post- synaptic stimulation corresponding to canonical experimental protocols used to induce synaptic plasticity (see Section 4). The parameters of this neuron model are matched to recent experimental data obtained at the CA3-CA1 synapse wherever available. Stimulation generates membrane depolarisation via backpropagating action potentials and conductance based synapses that exhibit short-term depression; as well as calcium influx through NMDA receptors (NMDAr-[Ca^{2+}]). Synaptic plasticity is governed by a Markov model, where stochastic transitions between binary high and low weight states proceed with dynamically evolving probabilities that we putatively associate with the activity of kinase and phosphatase pathways. These transition probabilities are non-zero at rest and modulated with distinct kinetics by calcium influx according to modified Hill functions that are inspired by recent advances in systems biology. The resultant change in total synaptic weight is averaged across ten trials in which identical stimulation protocols are applied to N=10000 homogeneous spines. This value can then be compared to the changes in excitatory post-synaptic currents or potentials recorded in empirical studies.

2.1 Dynamics of synaptic plasticity induction by spike-timing stimulation

Recent experiments conducted in acute hippocampal slices, which closely approximate the conditions present *in vivo*, have demonstrated that the plasticity of excitatory CA3-CA1 synapses is jointly dependent upon the temporal offset of pre- and post- synaptic firing, number of post-synaptic spikes fired, frequency of spike pairings, and duration of stimulation (Pike et al. 1999; Wittenberg and Wang 2006; Buchanan and Mellor 2007). Firstly, we aim to ascertain whether the calcium control hypothesis—which has been demonstrated to successfully reproduce earlier STDP data obtained in culture (Fig. 1a), as well as that induced by other activity patterns—can be revised to account for this joint dependency.

The experimental data we aim to replicate can be characterised by considering the effects of two different stimulation protocols—pairing 100 single pre- and post- synaptic spikes (hereafter referred to as 'spike pairing') at low frequencies (0.1–5 Hz), which generates a depression-only learning rule (Fig. 1b); or pairing a single pre-synaptic spike with two post-synaptic spikes (hereafter referred to as 'triplet pairing'), which generates a bidirectional, triphasic learning rule after 100 pairings at a frequency of 5 Hz (Fig. 1c), an unsaturated potentiation-only rule after 30 pairings at 5 Hz (Fig. 1d), or mild depression after 100 pairings at a frequency of 0.5 Hz (data not shown) (Pike et al. 1999; Wittenberg and Wang 2006). In the experimental literature, these learning curves are often fitted by a Gaussian or sum of Gaussians centred at short, positive temporal offsets, as illustrated in Fig. 1b-d (from (Wittenberg and Wang 2006)).

An examination of the simulated NMDAr-[Ca^{2+}] dynamics produced by these stimulation protocols illustrates the foundations for the calcium control hypothesis—high peak values generated by both spike and triplet pairings at short, predominantly positive temporal offsets and decaying exponentially with increasing temporal offset (Fig. 2a, b). Intuitively, setting arbitrary thresholds for kinase (θ_{LTP}) and phosphatase (θ_{LTD}) activation as the peak NMDAr-[Ca^{2+}] values achieved by spike pairings at short and long temporal offsets respectively will generate approximately Gaussian learning curves of different width centred at short positive temporal offsets that qualitatively replicate empirical data. We utilise these peak NMDAr-[Ca^{2+}] values to parameterize the threshold β_x of the Hill functions that control kinase and phosphatase activity, setting Hill coefficients and dissociation constants in line with previous experimental and theoretical studies, and accounting for the empirically observed competition between these two pathways by dictating that kinase activity partially inhibits phosphatase activity (see Section 4; (Fukunaga et al. 2000; Zhabotinsky 2000; Abarbanel et al. 2003; Pi and Lisman 2008)). Finally, we assign a higher gain and more rapid decay to the activation of kinase, such that LTP can be induced rapidly by a small number of spike or triplet pairings; while phosphatase activity accumulates slowly over time, such that significant LTD requires more sustained stimulation (Yang et al. 1999; Mizuno et al. 2001; Wittenberg and Wang 2006).

Constraining the dynamics of kinase and phosphatase activation in this way allows us to qualitatively replicate the full array of experimental data described above (Fig. 2c-f). The moderate peak NMDA-[Ca^{2+}] values produced by spike pairings delivered at low frequencies (i.e. 0.1–5 Hz) generate a depression only learning curve centred at short positive temporal offset (μ_D=22.7 ms) and extending over a wide range (σ_D=32.6 ms; Fig. 2c). Similar results are generated by triplet pairings delivered at low frequencies (i.e. 0.5 Hz; Fig. 2d). Conversely, triplet pairings at higher frequencies (i.e. 5 Hz) generate an unsaturated potentiation only learning rule centred at short positive temporal offsets (μ_P=19.85 ms) with a narrower range (σ_P=9.0 ms) when applied for short durations (Fig. 2e); and a triphasic learning rule (with μ_D=19.5, σ_D= 65.9 ms and μ_P=20.1, σ_P=9.5 ms) when applied for longer periods (Fig. 2f).

An examination of calcium, kinase, phosphatase and synaptic weight dynamics during 5 Hz triplet pairing provides further illustration of the mechanisms of this model (Fig. 3). Moderate elevations in intracellular calcium, generated here by acausal (i.e. post-pre) triplet pairings at 5 Hz, selectively activate phosphatase and subsequently increase

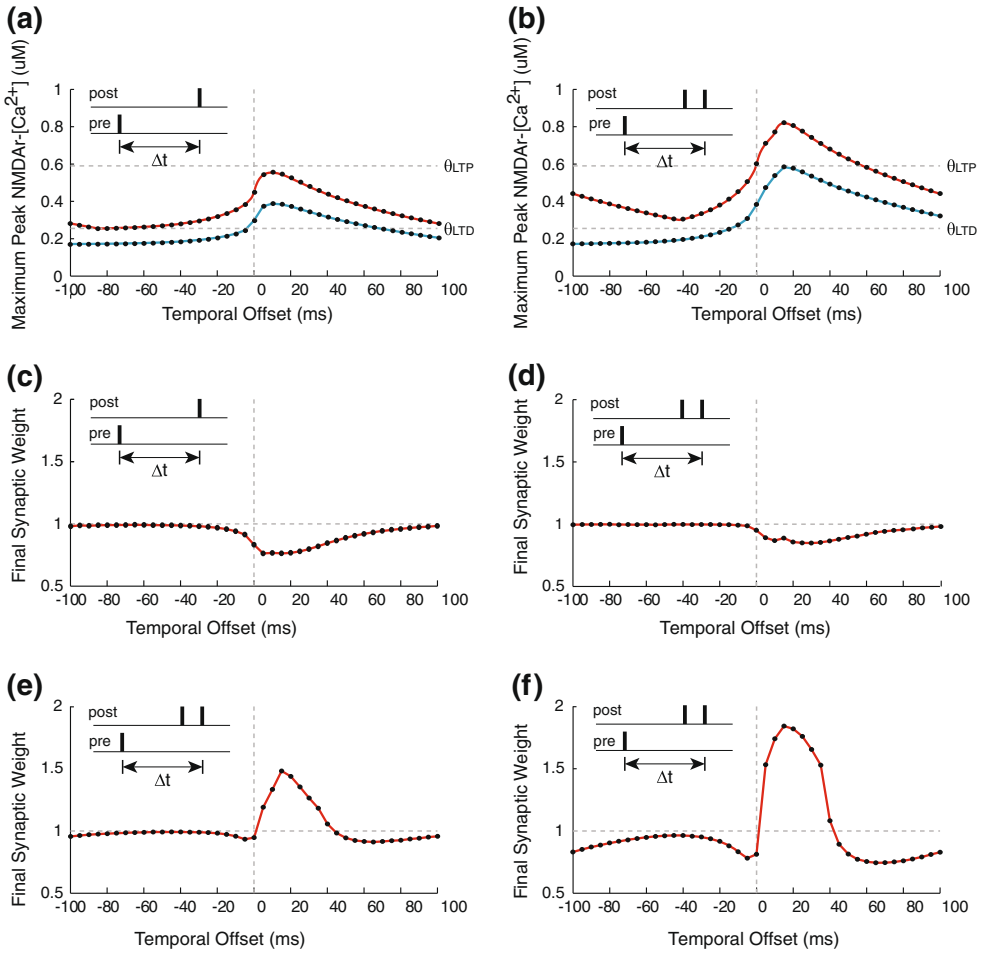

Fig. 2 NMDAr-[Ca^{2+}] and synaptic weight change generated by spike and triplet pairing stimulation protocols. **(a)** Maximum peak NMDAr-[Ca^{2+}] generated by 100 spike pairings delivered at 0.5 Hz (blue line) and 5 Hz (red line) with various temporal offsets ($\Delta t=t_{post}-t_{pre}$), $\tau_{bAP,s}=25$ ms and $\tau_{NMDA,s}=152$ ms. **(b)** Maximum peak NMDAr-[Ca^{2+}] generated by 30–100 triplet pairings delivered at 0.5 Hz (blue line) and 5 Hz (red line) with the same parameter values as (a). Horizontal dashed lines represent putative thresholds for the induction of LTP and LTD (θ_{LTP} and θ_{LTD} respectively) which are subsequently used to inform parameterisation of the thresholded Hill functions that control kinase and phosphatase activity respectively. Vertical dashed line represents $\Delta t=0$ ms. **(c)** Overall synaptic weight change generated by 100 spike pairings delivered at 5 Hz with $\tau_{bAP,s}=25$ ms, $\tau_{NMDA,s}=152$ ms, $\beta_P=0.39$, $\beta_D=0.175$, $k_P=0.04$ and $k_D=4\times10^{-4}$ when kinase and phosphatase dynamics are controlled by peaks in intracellular calcium concentration. Horizontal dashed line represents zero change in total synaptic weight. **(d)** Synaptic weight change generated by 100 triplet pairings delivered at 0.5 Hz with all other parameter values the same as (c). **(e)** Synaptic weight change generated by 30 triplet pairings delivered at 5 Hz with the same parameter values as (c). **(f)** Synaptic weight change generated by 100 triplet pairings delivered at 5 Hz with the same parameter values as (c)

the probability of synapses making the transition from high to low weight states. Conversely, more significant elevations in intracellular calcium, generated here by causal (i.e. pre-post) triplet pairings at 5 Hz, activate kinase and phosphatase pathways, the former inhibiting the latter and subsequently increasing the probability of synapses making the transition from low to high weight states. The higher gain of kinase activation dictates that the probability of transitions from low to high weight states is an order of magnitude greater during potentiating stimuli than the probability of transitions from high to low weight states during depressing stimuli (Fig. 3c, d). Subsequently, LTP is expressed more rapidly than LTD (mean transition times for potentiation and depression are 6.5±4.8 s and 11.0±5.8 s respectively for the 5 Hz triplet pairings illustrated in Fig. 3, for example). Finally, it is well known that relatively weak synaptic stimulation generates an early phase of potentiation or depression (E- LTP /LTD), primarily mediated by the (de-)phosphorylation of existing surface AMPAr, which subsequently decays over a period of hours. In contrast, stronger stimulation generates the same absolute magnitude of synaptic plasticity but also initiates *de novo* protein synthesis and changes in AMPAr trafficking which consolidate this weight change, such that it persists for a much longer period (Krug et al. 1984; Nguyen et al. 1994; Frey and Morris 1997). In these simulations, the decay of kinase and phosphatase activity to resting levels following

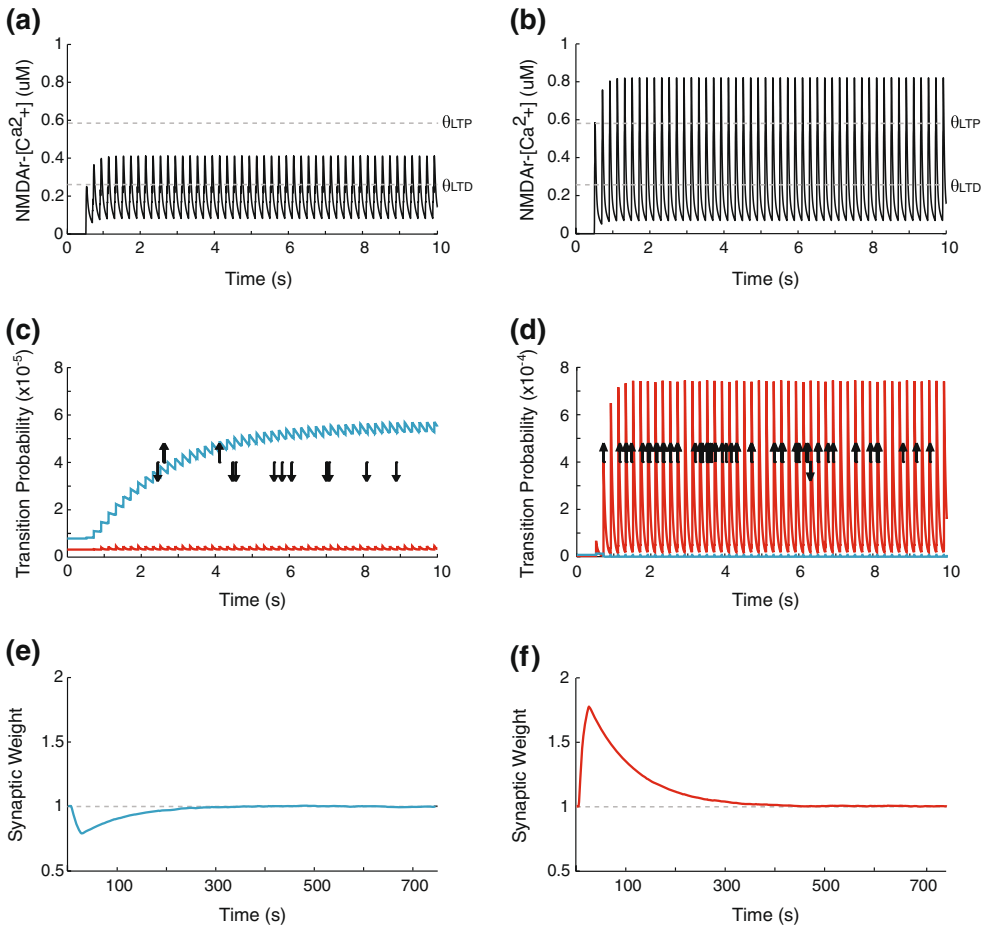

Fig. 3 Local dynamics of intracellular calcium, kinase and phosphatase activity and synaptic weight in the dendritic spine during potentiating and depressing causal and acausal spike pairings. **(a)** NMDAr-$[Ca^{2+}]$ dynamics in the dendritic spine during a typical depressing stimulus – 5 Hz triplet pairing with $\Delta t=t_{post}-t_{pre}=-15$ ms, $\tau_{bAP,s}=25$ ms and $\tau_{NMDA,s}=152$ ms. **(b)** NMDAr-$[Ca^{2+}]$ dynamics in the dendritic spine during a typical potentiating stimulus – 5 Hz triplet pairing with $\Delta t=t_{post}-t_{pre}=15$ ms and all other parameter values the same as (a). **(c)** Kinase (red) and phosphatase (blue) dynamics during the depressing stimulus illustrated in (a) with $\beta_P=0.39$, $\beta_D=0.175$, $k_P=0.04$ and $k_D=4\times10^{-4}$ when kinase and phosphatase dynamics are controlled by peaks in intracellular calcium concentration. Black arrows indicate the time of each observed transition between low and high weight states, or vice versa. **(d)** Kinase (red) and phosphatase (blue) dynamics during a typical potentiating stimulus with all other parameter values the same as (c). **(e)** Decay of LTD and **(f)** LTP following the potentiating and depressing stimulation protocols illustrated in (a-d)

stimulation dictates that the relative frequency of high and low synaptic weights returns to its initial distribution over a time course of ~1 h, in accordance with the decay of E- LTP / LTD observed empirically (Fig. 3e, f).

2.2 The range of temporal interactions, slow time constants and skew

The temporal extent of spike pair interactions at low frequencies is primarily determined by the slow time constant of the NMDA receptor, which dictates the duration of glutamate binding following pre-synaptic input; and the slower, less dominant component of the bAP, which dictates the duration of residual depolarisation and therefore partial relief of NMDA blockade in the spine following a post-synaptic action potential. It is therefore possible to indirectly infer the magnitude of these effective time constants from the weight change generated experimentally by STDP stimulation protocols. In the simulations described above, the slow time constant of the NMDA receptor ($\tau_{NMDA,s}=152$ ms) is much larger than that of the bAP ($\tau_{bAP,s}=25$ ms) and hence causal spike pair interactions extend over a larger temporal window. This accounts for the induction of depression over a greater range of positive than negative temporal offsets with spike pairing (Fig. 2c) or low frequency triplet pairing stimulation (Fig. 2d) and for the induction of more significant depression around $\Delta t=-100$ ms than $\Delta t=-50$ ms in high frequency triplet pairing simulations (Fig. 2f). In the latter case, it appears that post-synaptic bursts at large negative temporal offsets ($\Delta t<-50$ ms) interact more significantly with decaying NMDA receptor activation from the previous pre-synaptic input, as the 200 ms range of temporal offsets

illustrated here corresponds to a full stimulation cycle at 5 Hz (giving continuity at the end points of Fig. 2f). This appears to be quantitatively at odds with empirical data, which suggests that smaller net weight change should be generated as $\Delta t \rightarrow \pm 100$ ms for 5 Hz triplet pairing, and thus that consecutive triplet pairings should not interact at this stimulation frequency (Fig. 1c).

Independently modulating the relative magnitude of these slow time constants—without adjusting that of the dominant, fast component of the bAP—manipulates the positive and negative temporal extent, and thus the skew, of NMDAr-[Ca^{2+}] influx generated by spike or triplet pairings in this model (Fig. 4a, b). Simultaneously adjusting the Hill function thresholds for kinase and phosphatase activation allows the temporal extent and skew of the resultant learning curves to be similarly manipulated without significantly affecting the magnitude of LTD and LTP expressed (Fig. 4c, d). In order to better reflect the empirical data

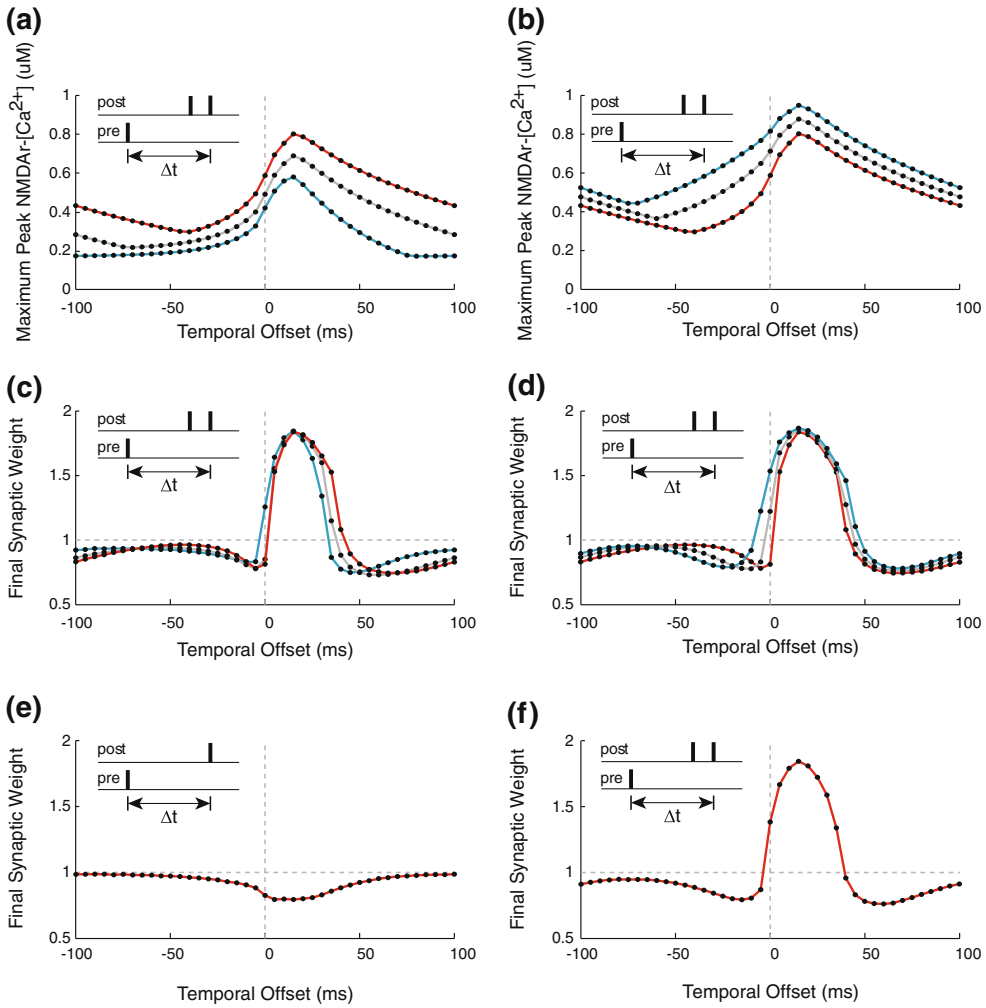

Fig. 4 Effects of adjusting NMDAr and bAP time constants on peak NMDAr-[Ca^{2+}] and synaptic weight change. **(a)** Peak NMDAr-[Ca^{2+}] values generated by 100 triplet pairings delivered at 5 Hz and various temporal offsets ($\Delta t = t_{post} - t_{pre}$) with $\tau_{bAP,s}=25$ ms and $\tau_{NMDA,s}=50$ ms (blue line); $\tau_{NMDA,s}=100$ ms (grey line); or $\tau_{NMDA,s}=152$ ms (red line). **(b)** Peak NMDAr-[Ca^{2+}] values generated by 100 triplet pairings delivered at 5 Hz with $\tau_{NMDA,s}=152$ ms and $\tau_{bAP,s}=25$ ms, (red line); $\tau_{bAP,s}=55$ ms (grey line); or $\tau_{bAP,s}=85$ ms (blue line). **(c)** Overall synaptic weight change generated by 100 triplet pairings delivered at 5 Hz with values of β_x adjusted such that the maximum amount of LTD and LTP expressed remains approximately constant; $\beta_P=0.175$ and $\beta_D=0$ (blue line); $\beta_P=0.28$ and $\beta_D=0.07$ (grey line); $\beta_P=0.39$ and $\beta_D=0.175$ (red line). In each case, $k_P=0.04$, $k_D=4\times10^{-4}$, kinase and phosphatase dynamics are controlled by peaks in intracellular calcium concentration, and all other parameter values are the same as in (a). **(d)** Synaptic weight change generated by 100 triplet pairings delivered at 5 Hz with values of β_x adjusted such that the maximum amount of LTD and LTP expressed remains approximately constant; $\beta_P=0.39$ and $\beta_D=0.175$ (red line); $\beta_P=0.45$ and $\beta_D=0.24$ (grey line); $\beta_P=0.51$ and $\beta_D=0.31$ (blue line). In each case, $k_P=0.04$, $k_D=4\times10^{-4}$, kinase and phosphatase dynamics are controlled by peaks in intracellular calcium concentration, and all other parameter values are the same as in (b). **(e)** Synaptic weight change generated by 100 spike pairings delivered at 5 Hz with $\tau_{bAP,s}=55$ ms, $\tau_{NMDA,s}=100$ ms, $\beta_P=0.32$, $\beta_D=0.125$, $k_P=0.04$ and $k_D=4\times10^{-4}$, where kinase and phosphatase dynamics are controlled by peaks in intracellular calcium concentration. **(f)** Synaptic weight change generated by 100 triplet pairings delivered at 5 Hz with the same parameter values as (e)

illustrated in Fig. 1b, c—by extending the temporal range of acausal spike pair interactions and reducing that of causal interactions, as well as increasing the negative skew of the NMDAr-[Ca^{2+}] profile and resultant learning curves—we therefore repeat the simulations described above with $\tau_{bAP,s}$=55 ms and $\tau_{NMDA,s}$=100 ms (Fig. 4e, f). This represents a significantly larger slow time constant for the bAP than that employed in previous modelling studies; although there is little empirical data available to guide the choice of this parameter value (Shouval et al. 2002; Rackham et al. 2010; Stuart and Sakmann 1994; Magee and Johnston 1997; Larkum et al. 2001). The slow time constant of calcium influx through the NMDA receptor is also shorter than that measured experimentally, which has been shown to correspond well with the time course of receptor deactivation following glutamate release (~150 ms; (Sabatini et al. 2002)). However, that study measured the time course of calcium influx following unitary NMDAr activation, as oppose to NMDAr kinetics when significant post-synaptic depolarisation follows glutamate binding by ~50–100 ms, for which no empirical data is available. We use this combination of slow time constants in all further simulations presented here, but it is important to note that each of the results described can be qualitatively replicated with $\tau_{bAP,s}$=55 ms and $\tau_{NMDA,s}$=152 ms, as employed in the vast majority of previous theoretical studies (Supplementary Figure 1).

2.3 Induction of synaptic plasticity by tetanic stimulation

Having constrained the parameters of the plasticity model to account for recent observations of triphasic hippocampal STDP, we now examine whether it is also possible to replicate synaptic plasticity data obtained using other stimulation protocols in order to provide a unified account of dynamic weight change dictated by NMDAr-[Ca^{2+}]. Firstly, we examine tetanic stimulation—whereby a set number of pre-synaptic inputs are applied periodically at a constant firing rate (see Section 4). This form of stimulation typically generates a Bienenstock, Cooper and Munro (1982) or 'BCM' type learning curve, illustrated in Fig. 5a (Bienenstock et al. 1982). Conversely, in our simulations, only LTD is generated across the same range of input firing rates. Closer examination reveals that this results from the inclusion of short-term synaptic depression, with a more recognizable BCM-type curve being generated when simulations are repeated in the absence of short-term plasticity (i.e. with F_D=0, see Section 4; Fig. 5b). However, the firing rate at which LTD and LTP are first expressed in these simulations remains significantly higher than that observed experimentally (O'Connor et al. 2005b).

One issue with the interpretation of empirical plasticity data obtained using tetanic stimulation protocols is the fact that post-synaptic activity is rarely recorded, but has a significant impact on the magnitude of NMDAr-[Ca^{2+}] generated. In fact, experimental evidence suggests that post-synaptic activity is a necessary requirement for any form of synaptic plasticity, although contradictory reports do exist (Shouval et al. 2010; Christie et al. 1996; Fan et al. 2005). Wittenberg and Wang (Wittenberg and Wang 2006) provide unique data regarding the induction of LTD by a single LFS protocol (900 pulses at 3.3 Hz), in that the response of the post-synaptic neuron was recorded throughout pre-synaptic stimulation—as 200 action potentials which each followed input volleys with a latency of 6.2±4 ms. Previous computational models of STDP are likely to translate these repeated causal spike pairings into LTP, in contrast with this empirical data, highlighting a critical weakness of those models (Shouval et al. 2010). In contrast, when we apply tetanic stimulation in the presence of stochastic post-synaptic activity with the same statistics, then a BCM-type learning rule with realistic thresholds for the expression of both LTD and LTP is generated, both with and without short-term synaptic depression (Fig. 5c). Again, the expression of LTP is much more rapid than that of LTD during tetanic stimulation (the average transition from low→high weight taking place 13±7 s after the onset of 50 Hz stimulation, and the average high→low weight transition taking place 120±76 s after the onset of 5 Hz stimulation) and on a similar timescale to that observed experimentally (80±70s for LTP and 183±126 s for LTD in O'Connor, Wittenberg and Wang (O'Connor et al. 2005a); 38 s for LTP in Bagal et al. (Bagal et al. 2005)). Moreover, all changes in synaptic strength subsequently decay over a period of hours.

The modified Hill functions that control kinase and phosphatase dynamics in this model also allow the NMDAr-[Ca^{2+}] threshold at which potentiation and depression are expressed to be modulated in a straightforward manner (see Section 4). Thus, a process of metaplasticity—whereby the level of tetanic stimulation required to induce LTP / LTD is dynamically modified by ongoing synaptic activity—can easily be incorporated (Morgan 2007; Buchler and Cross 2009). For example, increasing the threshold for kinase activation β_P shifts the position of the theoretical modification threshold to higher firing rates (Fig. 5d). Furthermore, setting the gain of kinase or phosphatase activation k_x=0 reveals the competitive and co-activated processes of potentiation and depression observed experimentally under selective pharmacological blockade (Fig. 5e, f).

2.4 Induction of synaptic plasticity by other stimulation protocols

Finally, we examine the dynamics of synaptic plasticity generated by a variety of other stimulation protocols. Firstly, we pair pre-synaptic stimulation with different levels of post-synaptic depolarisation, a protocol that has

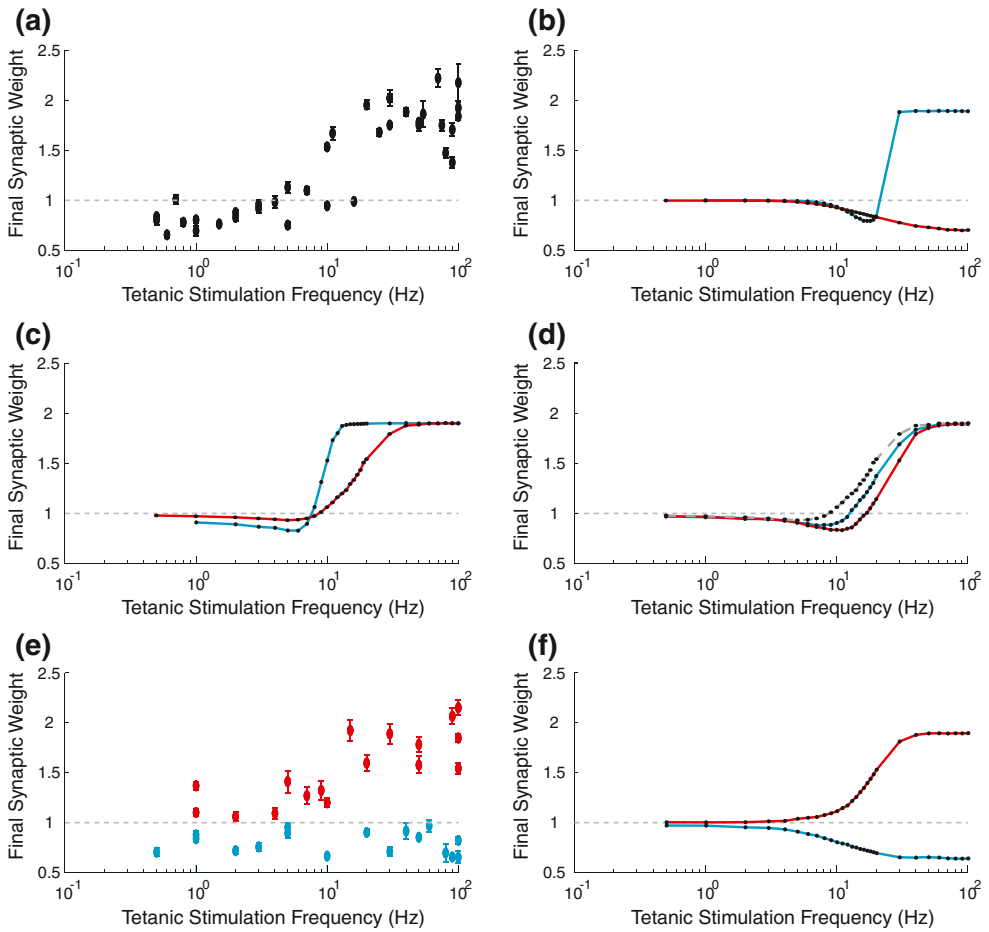

Fig. 5 Synaptic plasticity induced by tetanic stimulation. **(a)** Experimentally observed synaptic weight change induced by periodic pre-synaptic stimulation delivered at various firing rates from (O'Connor et al. 2005b). **(b)** Overall synaptic weight change generated in the model when the same form of stimulation is applied with $\tau_{bAP,s}$=55 ms, $\tau_{NMDA,s}$=100 ms, β_P=0.32, β_D=0.125, k_P=0.04 and k_D=4×10^{-4}, kinase and phosphatase dynamics controlled by peaks in intracellular calcium concentration, in the presence (red line) or absence (blue line) of short-term synaptic depression. **(c)** Overall synaptic weight change generated in the model by periodic pre-synaptic stimulation delivered at various firing rates in the presence of stochastic post-synaptic activity that follows the statistics described in (Wittenberg and Wang 2006) and all other parameter values the same as in (b). **(d)** Overall synaptic weight change generated in the model by periodic pre-synaptic stimulation delivered at various firing rates in the presence of stochastic post-synaptic activity that follows the statistics described in (Wittenberg and Wang 2006) with short-term synaptic depression, β_P=0.37 (blue line) or β_P=0.42 (red line) and all other parameter values the same as in (c). **(e)** Experimentally observed weight change induced by periodic pre-synaptic stimulation delivered at various firing rates in the presence of selective pharmacological blockade of kinase (blue) or phosphatase (red) activity from (O'Connor et al. 2005b). **(f)** Overall synaptic weight change generated in the model when the same form of stimulation is applied under conditions of putative kinase (blue) or phosphatase (red) blockade (i.e. k_P=0 or k_D=0), with short-term depression, and all other parameter values the same as in (b)

been empirically demonstrated to produce a BCM-type curve, with LTD at moderate post-synaptic membrane voltages giving way to LTP at higher levels of depolarisation due to the increasing influx of calcium through the voltage gated NMDA receptor (Ngezahayo et al. 2000). This data is well replicated by the model (Fig. 6a). Next, we examine the impact of manipulating the amplitude of the bAP during triplet pairing stimulation. It is well known that bAP amplitude attenuates significantly with distance from the soma, reducing the voltage-dependent relief of NMDAr following a post-synaptic action potential, and this may have a critical impact on the nature of synaptic weight change generated by identical stimulation protocols at proximal and distal dendrites (Larkum et al. 2001; Johnston et al. 2003; Canepari et al. 2007). Simulations indicate that a reduction in the value of $V_{bp,max}$ generates a reduction in the magnitude of LTP and the temporal extent of both LTP and LTD generated by triplet pairing protocols (Fig. 6b). This matches recent experimental data from cortical pyramidal neurons—although similar results from CA1 pyramidal neurons are so far lacking (Froemke et al. 2005).

Next, we examine the change in synaptic weight generated by approximately synchronous pre- and post- synaptic bursts delivered with differing intra-burst frequency. In the acute cortical slice, this form of stimulation has been applied to

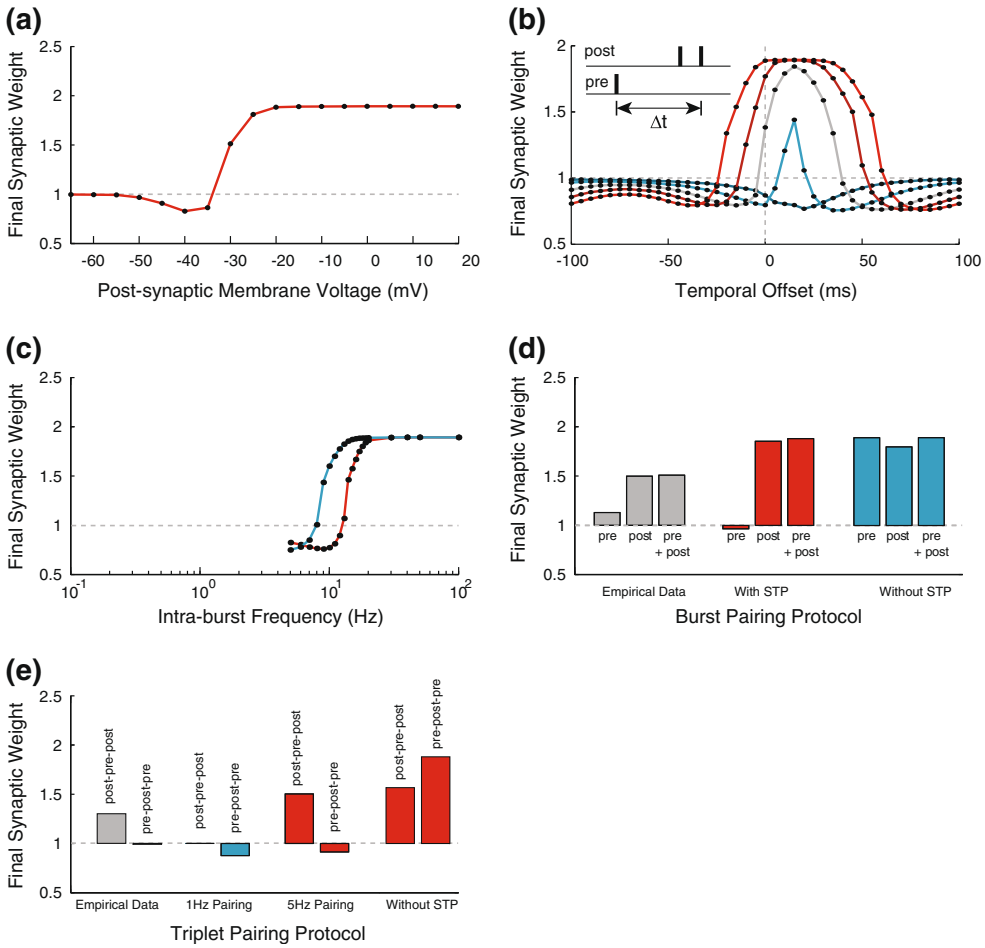

Fig. 6 Synaptic plasticity induced by other stimulation protocols. **(a)** Overall synaptic weight change generated by 100 pre-synaptic inputs delivered at 2 Hz while the post-synaptic membrane voltage is held fixed at various levels of depolarisation, with $\tau_{bAP,s}$=55 ms, $\tau_{NMDA,s}$= 100 ms, β_P=0.32, β_D=0.125, k_P=0.04 and k_D=4×10^{-4} , where kinase and phosphatase dynamics are controlled by peaks in intracellular calcium concentration. **(b)** Synaptic weight change generated by 100 triplet pairings delivered at 5 Hz with various temporal offsets ($\Delta t=t_{post}-t_{pre}$), $V_{bp,\ max}$=33 mV (blue line), $V_{bp,\ max}$=50 mV, $V_{bp,\ max}$=67 mV (grey line), $V_{bp,\ max}$=83 mV and $V_{bp,\ max}$=100 mV (red line) and all other parameters the same as in (a). **(c)** Synaptic weight change generated by forty causal (blue) and acausal (red) pre- and post- synaptic bursts delivered at 0.5 Hz with differing intra-burst frequency and all other parameters the same as in (a). **(d)** Synaptic weight change generated by 10 causal pre- and / or post- synaptic burst pairings delivered at 5 Hz in the experimental data from (Pike et al. 1999) (grey) and in the model with (red) and without (blue) short-term synaptic depression, where all other parameters are the same as in (a). **(e)** Synaptic weight change generated by 60 triplet pairings delivered at 1 Hz in the experimental data from (Wang et al. 2005) (grey) and in the model at 1 Hz (blue) and 5 Hz (red), with and without short-term synaptic depression, where all other parameters are the same as in (a)

demonstrate that the degree and direction of synaptic weight change induced by temporally correlated pre- and post- synaptic activity is highly dependent on the temporal proximity of consecutive spike pairings, with LTD induction at low intra-burst frequencies giving way to LTP induction at higher intra-burst frequencies (Sjöström et al. 2001; Froemke et al. 2006). This experimental data can again be characterized by a BCM-type curve that is well replicated by the model (Fig. 6c).

Further experiments in acute hippocampal slices have demonstrated that the induction of LTP is explicitly dependent upon post-synaptic bursting, but relatively insensitive to the number of pre-synaptic spikes (Pike et al. 1999; Larson et al. 1986; Frick et al. 2004). Again, this data is well replicated by the model, with solely pre-synaptic bursting generating no significant weight change, while post-synaptic bursting is sufficient to induce LTP when paired with one or more pre-synaptic spikes (Fig. 6d). Complementary data from cortical preparations suggest that the failure of multiple pre-synaptic spikes to induce LTP may be attributed—at least, in part—to the short-term depression of transmitter release (Froemke et al. 2006). Accordingly, when these simulations are repeated in the absence of short-term depression, an approximately equal magnitude of LTP is incurred by pre-synaptic bursts paired with single post-synaptic action potentials and single pre-synaptic action potentials paired with post-synaptic bursts.

Similar experimental investigations in hippocampal cultures have examined the synaptic weight change generated by more elaborate triplet pairings. These studies revealed an apparent asymmetry in the temporal integration of potentiation and depression processes (Froemke et al. 2006; Rubin et al. 2005; Wang et al. 2005). Specifically, LTP is expressed if a causal spike pairing follows an acausal spike pairing with approximately equal temporal offset; but no significant weight change is induced if the order of spike pairings is reversed. At first examination, it appears that the model is unable to account for this data, as moderate LTD is generated by both pre-post-pre and post-pre-post pairings (Fig. 6e). However, it is important to note that there is a discrepancy between that data, obtained from hippocampal cultures, and the results illustrated in Fig. 1b-d, which are acquired from the acute slice, as causal triplet pairings delivered at 1 Hz induce significant LTP in culture but mild LTD in the slice (Wittenberg and Wang 2006; Wang et al. 2005). When we increase the frequency of triplet pairings to 5 Hz, then the degree and direction of weight change observed in culture is qualitatively replicated by the model. Again, these results are dependent on the inclusion of short-term synaptic depression—when this feature of the model is removed, then a greater level of potentiation is incurred by pre-post-pre pairings (Fig. 6e).

Finally, we demonstrate that each of the results described above can be replicated when the dynamics of kinase and phosphatase activity are controlled by integrated calcium influx (see Section 4). Figure 7 illustrating the synaptic weight change generated by spike and triplet pairing, tetanic, post-synaptic depolarisation and burst pairing stimulation protocols. In each case, the results are comparable both to experimental findings and to the less computationally demanding case where plasticity is controlled solely by local peaks in NMDAr-$[Ca^{2+}]$. Importantly, the inclusion of short-term synaptic depression is still required to replicate certain aspects of empirical plasticity data in this case (Fig. 7e, f).

3 Discussion

Recent empirical examinations of spike-timing dependent plasticity at the CA3-CA1 synapse have demonstrated that changes in synaptic conductance are jointly dependent on the temporal offset of pre- and post- synaptic firing, number of post-synaptic spikes fired, frequency of spike or triplet pairings and duration of stimulation (Pike et al. 1999; Wittenberg and Wang 2006; Buchanan and Mellor 2007). We have demonstrated that the calcium control hypothesis—which has previously shown that peak NMDAr-$[Ca^{2+}]$ influx is sufficient to account for the spike-timing dependence of triphasic hippocampal plasticity—can be extended to incorporate the influence of post-synaptic bursting, stimulus duration, frequency, and the dynamic nature of step-like changes between binary synaptic states. Our motivation was to reproduce a wide range of plasticity data using a minimal number of assumptions and thereby provide a parsimonious model that is suitable for network level simulations (Shouval et al. 2002; Graupner and Brunel 2010). In addition to those made previously, we have incorporated co-activated and competitive kinase and phosphatase pathways with distinct kinetics that dictate probabilistic transitions in a Markov model of binary synaptic states. We have demonstrated that the frequency dependent accumulation of NMDAr-$[Ca^{2+}]$ is sufficient to account for the frequency dependence of hippocampal STDP; assigning more rapid kinetics to the kinase pathway responsible for potentiating weight transitions is sufficient to account for the shorter duration of stimulation required to induce LTP; the use of binary synaptic weight states dictates that the magnitude of LTP and LTD naturally saturates, avoiding the need for ad-hoc limits on maximum weight change; and assigning non-zero equilibrium values to kinase and phosphatase activation is sufficient to replicate the decay of early phase plasticity. We have subsequently demonstrated that this plasticity model can replicate experimental data obtained using a number of stimulation protocols. In summary, we provide a parsimonious, unified computational model of synaptic plasticity at connections between excitatory hippocampal neurons—a process that is critically implicated in mammalian declarative memory function—with particular emphasis on the dynamics of synaptic weight change.

We have utilised this model to make two predictions regarding the dynamics of NMDAr-dependent calcium influx generated by STDP stimulation protocols. Firstly, we suggest that the induction of LTD by post-pre spike pairings over a range of -60 ms$<\Delta t<$0 ms implies that the slow, less dominant component of the bAP (dictated in these simulations by the parameter $\tau_{bAP,s}$) should follow a similar time course in dendritic spines, although it is very difficult to test this conjecture experimentally. Secondly, in order to avoid spurious pre-post pairings at $\Delta t>\sim$60 ms, the NMDA receptor should not allow significant calcium influx when depolarisation follows glutamate binding by a similar temporal offset. This prediction could be tested through experimental measurements of the NMDAr-$[Ca^{2+}]$ current generated by spike and triplet pairing protocols at different stimulation frequencies. It is also well known that activity-dependent NR2A / NR2B subunit composition has a significant influence on the temporal profile of NMDAr currents, particularly at the high and low firing rates associated with synaptic plasticity induction (Erreger et al. 2005; Perez-Otano and Ehlers 2005; Gerkin et al. 2007). Moreover, it has been demonstrated that these subunits independently

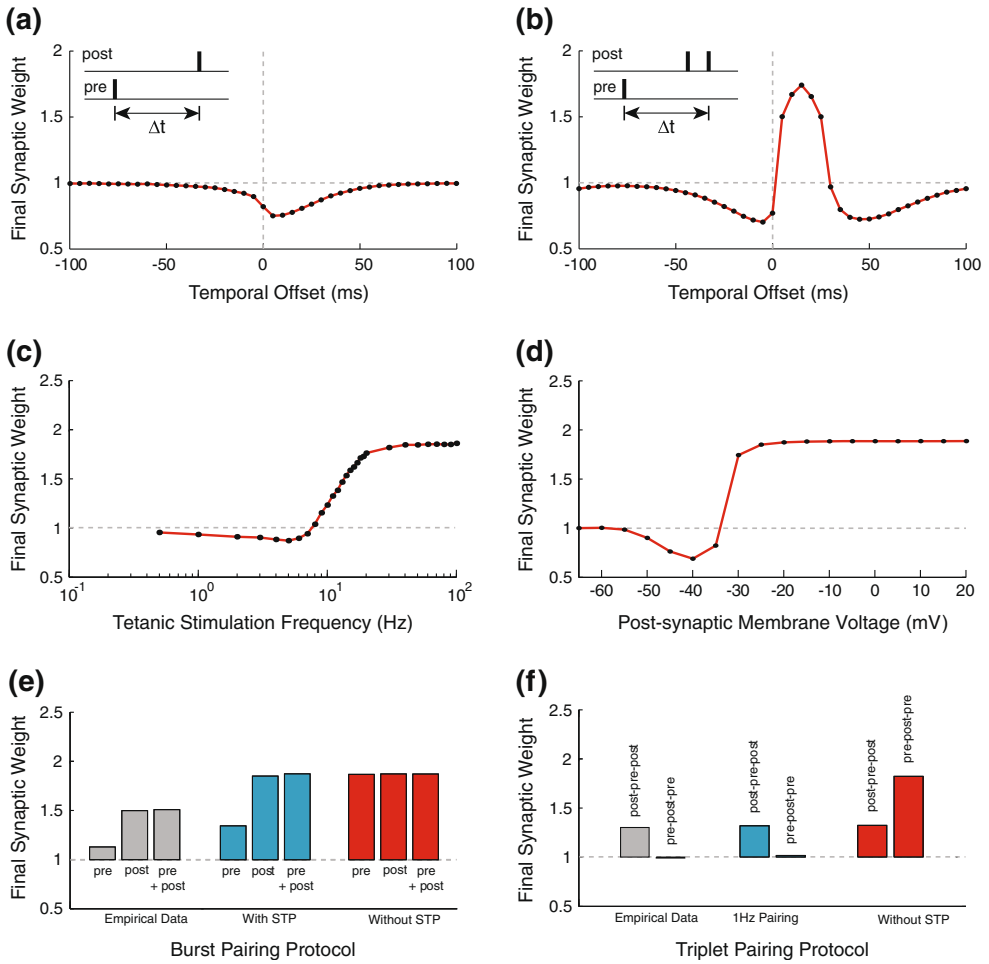

Fig. 7 Summary of synaptic plasticity data generated by integrated calcium influx. **(a)** Overall synaptic weight change generated by 100 spike pairings delivered at 5 Hz with $\tau_{bAP,s}$=55 ms, $\tau_{NMDA,s}$=100 ms, β_P=0.32, β_D=0.125, $k_P=1\times10^{-3}$ and $k_D=4\times10^{-6}$, where kinase and phosphatase dynamics are controlled by integrated calcium influx. Horizontal dashed line represents zero change in total synaptic weight. **(b)** Synaptic weight change generated by 100 triplet pairings delivered at 5 Hz with all other parameter values the same as in (a). **(c)** Synaptic weight change generated by tetanic pre-synaptic stimulation delivered at various firing rates in the presence of stochastic post-synaptic activity that follows the statistics described in (Wittenberg and Wang 2006), and all other parameter values the same as in (a). **(d)** Synaptic weight change generated by 100 pre-synaptic inputs delivered at 2 Hz while the post-synaptic membrane voltage is held fixed at various levels of depolarisation, and all other parameter values the same as in (a). **(e)** Synaptic weight change generated by 10 causal pre- and / or post- synaptic burst pairings delivered at 5 Hz in the experimental data from (Pike et al. 1999) (grey) and in the model with (blue) and without (red) short-term synaptic depression, where all other parameters are the same as in (a). **(f)** Synaptic weight change generated by 60 triplet pairings with various temporal offsets delivered at 1 Hz in the experimental data from (Wang et al. 2005) (grey) and in the model with (blue) and without (red) short-term synaptic depression, where all other parameters are the same as in (a)

mediate spike-timing dependent potentiation and depression (tLTP / tLTD) in hippocampal cultures and may subsequently control the temporally asymmetric integration of those processes revealed by triplet and quadruplet pairing experiments (Rubin et al. 2005; Wang et al. 2005; Gerkin et al. 2007).

The dynamics of kinase and phosphatase activation in this model are dictated by modified Hill functions inspired by recent advances in systems biology (Morgan 2007; Buchler and Cross 2009). These functions were developed to provide a quantitative kinetic description of enzymes and transcription factors that are sequestered by inhibitors or antagonists into inactive complexes below some threshold or equivalence point. This sequestration mechanism, widespread in genetic and regulatory networks, has several properties that make it particularly useful for modelling synaptic plasticity processes, providing a threshold for activation below which the accumulation of active regulatory molecules is effectively buffered and above which an ultrasensitive response that approaches bistability is generated. It is also straightforward to parameterise these modified Hill functions to suit the demands of any particular synaptic

plasticity simulation, by matching the threshold value β_x to the peak NMDAr-[Ca^{2+}] values generated by different forms of stimulation at which the expression of potentiation or depression is required, or dynamically modulate these thresholds to implement a process of metaplasticity.

It is important to note that the results presented here are only intended to model long-term plasticity of CA3-CA1 synapses in the hippocampus. Experimental studies have highlighted several important distinctions between the properties and mechanisms of plasticity at cortical and hippocampal synapses, indicating that a single theoretical formulation is insufficient to account for both, and it is tempting to speculate that this dichotomy might both reflect and be reflected by functional differences in neural processing mediated by these regions (Song et al. 2000). For example, although it is clear that buffering of post-synaptic calcium during stimulation prevents LTP and LTD in both hippocampal and cortical preparations, the triphasic STDP rule described here has only been observed in hippocampal preparations, while all studies of cortical synapses have revealed a biphasic STDP rule of the type illustrated in Fig. 1a (Wittenberg and Wang 2006; Sjöström et al. 2001; Froemke et al. 2006; Froemke et al. 2005; Gerkin et al. 2007). The calcium control hypothesis naturally generates a triphasic window due to the intermediate calcium concentrations produced by causal spike pairings at longer temporal offsets, and this makes the biphasic STDP learning curve difficult to explain by a naïve calcium control model alone. Previous computational modeling studies have presented a variety of putative mechanisms for avoiding LTD at longer positive temporal offsets—by incorporating stochasticity, dynamic interactions that veto depression following a causal spike pairing, or segregating the induction mechanisms of LTD and LTP (Karmarkar and Buonomano 2002; Shouval and Kalantzis 2005; Rubin et al. 2005; Graupner and Brunel 2007; Urakubo et al. 2008). In support of the latter approach, recent empirical data suggests that tLTD induction at cortical synapses relies on pre-synaptic NMDAr activation and retrograde cannabinoid signalling, as well as being at least partially dependent on the activation of metabotropic glutamate receptors and voltage-gated calcium channels (Froemke et al. 2006; Sjöström et al. 2003; Bender et al. 2006; Nevian and Sakmann 2006; Rodríguez-Moreno and Paulsen 2008). Conversely, there is little evidence to suggest that hippocampal synaptic plasticity is as strongly dependent on these mechanisms.

This situation is confused, however, by the fact that biphasic STDP has also frequently been observed in hippocampal cultures (Bi and Poo 1998; Wang et al. 2005). One possible explanation is that LTD generated by longer positive temporal offsets is a product of feed-forward inhibition, which is insignificant in hippocampal cultures but present in the acute slice (Nishiyama et al. 2000). This hypothesis gains some support from a study which demonstrated that LTD induced at longer positive temporal offsets can be selectively eliminated by bath application of the GABAergic antagonist bicuculline (Aihara et al. 2007). However, conflicting results come from whole cell recordings carried out in bath application of the GABAergic antagonist picrotoxin, which reveal no significant effect on the existence or profile of the second tLTD window (Wittenberg and Wang 2006). There are a number of other significant differences in synapse number, strength and development between acute slices and cell cultures that can have a significant effect on the induction of synaptic plasticity, and may therefore be responsible for the apparent existence of a triphasic STDP curve in the slice and biphasic curve in culture (Bi and Poo 1998; Buchanan and Mellor 2007; Meredith et al. 2003; Aihara et al. 2007). Whatever the relative contribution of inhibitory input to the profile of the triphasic STDP window, it is well known that CA1 pyramidal neurons receive predominantly inhibitory input from multiple sources during stereotyped learning and spatial exploration *in vivo*, and that changes in the level of inhibition during development significantly modulate the degree and direction of synaptic plasticity incurred by spike-timing stimulation protocols (Buchanan and Mellor 2007; Meredith et al. 2003). Hence, it seems prescient to extend this model to include realistic patterns of inhibitory input, in order to provide a more comprehensive appraisal of synaptic plasticity at the CA3-CA1 synapse.

The model presented here exhibits several further limitations that might be addressed by future theoretical studies. For example, several experimental results can only be replicated here by the inclusion of short-term synaptic depression, but it is unlikely that this represents the sole mechanism responsible for the lack of LTP induced by multiple pre-synaptic spikes *in vivo* (Froemke et al. 2006). The magnitude of weight change induced by different stimulation protocols in this model is also generally smaller than that observed empirically, despite the fact that the relative frequency of occurrence and conductance of potentiated and depressed synapses are matched to published data (Petersen et al. 1998; O'Connor et al. 2005a; Abarbanel et al. 2005). Moreover, AMPAr and NMDAr conductances are not linked to changes in putative synaptic strength, such that the magnitude of depolarisation generated by synaptic currents is equal for high and low weight synapses—i.e. synapses do not generate larger synaptic currents, and therefore greater depolarisation in the spine, following LTP. Although this is in line with the vast majority of theoretical studies of plasticity induction, is clearly at odds with the situation *in vivo* ((Shouval et al. 2002; Pfister and Gerstner 2006; Sjöström et al. 2008; Zhabotinsky 2000; Karmarkar and Buonomano 2002; Abarbanel et al. 2003; Shouval and Kalantzis 2005; Abarbanel et al. 2005; Rubin et al. 2005; Graupner and

Brunel 2007; Pi and Lisman 2008; Urakubo et al. 2008), for reviews see (Rackham et al. 2010; Graupner and Brunel 2010)). It has also been demonstrated that changes in AMPAr conductance associated with the expression of long-term synaptic plasticity are accompanied by concomitant changes in NMDAr conductance (Perez-Otano and Ehlers 2005; Watt et al. 2004). This has interesting implications for further synaptic plasticity—as both the level of depolarisation in the spine and the level of NMDAr-dependent calcium influx generated by that depolarisation will be concurrently modulated, possibly contributing to the 'lock-in' of changes in synaptic conductance observed experimentally (O'Connor et al. 2005a). By elaborating the secondary messenger pathways in the plasticity model to more closely replicate the activity of CaM, CaMKII, PP1, PP2A, I1 and other proteins implicated in plasticity expression, as well as additional sources of internal and external calcium influx, it may be possible to more accurately appraise the mechanisms of synaptic plasticity (Citri and Malenka 2008; Graupner and Brunel 2007; Lisman and Spruston 2005). However, the complexity of such models and associated computational cost might also render them unsuitable for network level simulation.

Finally, it is well established that processes of synaptic plasticity are accompanied by concurrent and interacting processes of homeostatic and intrinsic plasticity which regulate neural activity over longer timescales (Nelson and Turrigiano 2008; Desai 2003). Recent computational modelling suggests that the interaction of these processes is critical to establish and maintain appropriate conditions for transient dynamics during cognitive processing, and the examination of a unified model of neural and synaptic plasticity is therefore a critical direction for future theoretical studies (Buonomano 2005; Lazar et al. 2009; Buzsáki 2010; Fiete et al. 2010). More generally, an examination of the synaptic and neural dynamics generated by the triphasic STDP rule in network models of hippocampal function with realistic activity patterns, including theta modulation and phase precession, would contribute significantly to the understanding of hippocampal function during putative learning behaviour (Bush et al. 2010). The requirement for multiple post-synaptic spikes to induce LTP, for example, implies that bursting may be the primary mode of encoding salient information in the hippocampus (Lisman 1997; Harris et al. 2001). The distribution of inhibitory and excitatory inputs with different properties at different locations across the dendritic tree will generate more complex patterns of post-synaptic depolarisation and calcium influx, possibly allowing useful nonlinear computations to be performed. Recent studies have described several forms of heterosynaptic plasticity in pyramidal neurons that might also be explained by the calcium control hypothesis, allowing the nature of active dendritic processing to be more precisely elucidated (Dudman et al. 2007; Kampa et al. 2007; Losonczy et al. 2008; Legenstein and Maass 2011).

4 Methods

4.1 Neuron model

The vast majority of afferent excitatory synapses on cortical pyramidal neurons are found on dendritic spines—small, membranous protrusions that are connected to the dendritic tree by a narrow neck (Harris and Kater 1994). Due to the limited diffusion of biochemical signals including calcium through this neck, dendritic spines effectively compartmentalise synaptic processes and thereby promote their independence (Larkum et al. 2001). In this model, we examine N independent, passive dendritic spines with surface area A_{spine} whose membrane potential V_N (mV) is dictated solely by leak conductance according to Eq. (1); where C_m is the specific membrane capacitance, I_N (mA) is the total synaptic current to the Nth spine, g_L is the maximum leak conductance and E_L is the reversal potential of the leak current.

$$\frac{dV_N}{dt} = \frac{1}{C_m}\left(\frac{I_N}{A_{spine}} - \overline{g}_L(V_N - E_L)\right) \tag{1}$$

Each spine has AMPA and NMDA mediated synaptic currents with kinetics based on experimental recordings and governed by Eq. (2); where $\overline{g}_{\frac{AMPA}{NMDA}}$ represents the maximum conductance, $P_{AMPA/NMDA}$ the dimensionless open channel probability and $E_{AMPA/NMDA}$ the reversal potential (Destexhe et al. 1994; Dayan and Abbott 2001). Following an incoming action potential at time t_0, AMPAr conductance is modelled as a single exponential with instantaneous rise time and subsequent decay with a time constant of τ_{AMPA}=5.26 ms; while NMDAr conductance is modelled as the sum of fast and slow exponentials with time constants $\tau_{NMDA,rise}$=1.5 ms and $\tau_{NMDA,s}$ varying between 50 ms and 152 ms respectively (Dayan and Abbott 2001). The term B_{NMDA} is a normalisation factor which ensures that the peak conductance generated by this alpha function remains equal to the maximum conductance when the individual time constants are adjusted, while G_{NMDA} describes the additional voltage dependence due to the blockade of NMDA receptors by Mg^{2+} (Dayan and Abbott 2001; Jahr and Stevens 1990). Finally, each synapse exhibits short-term depression, such that the dimensionless probability of release is reduced immediately after pre-synaptic glutamate release, and subsequently returns to its equilibrium value P_0=0.5 with a time constant of τ_{rel}=50 ms (Dayan and Abbott 2001).

$$
\begin{aligned}
I_N &= I_{AMPA} + I_{NMDA} \\
I_{AMPA} &= -\overline{g}_{AMPA} P_{AMPA} (V_N - E_{AMPA}) \\
P_{AMPA}(t) &= P_{rel} \exp^{(t_0 - t)/\tau_{AMPA}} \\
I_{NMDA} &= -\overline{g}_{NMDA} P_{NMDA} G_{NMDA} (V_N - E_{NMDA}) \\
P_{NMDA}(t) &= P_{rel} B_{NMDA} \left(\exp^{(t_0 - t)/\tau_{NMDAs}} - \exp^{(t_0 - t)/\tau_{NMDAf}} \right) \\
B_{NMDA} &= \left(\left(\frac{\tau_{NMDAf}}{\tau_{NMDAs}} \right)^{\frac{\tau_{NMDArise}}{\tau_{NMDAs}}} - \left(\frac{\tau_{NMDAf}}{\tau_{NMDAs}} \right)^{\frac{\tau_{NMDArise}}{\tau_{NMDAf}}} \right)^{-1} \\
G_{NMDA} &= \frac{1}{\left(1 + \frac{[Mg^{2+}]}{3.57} \exp^{-V_N/16.13} \right)} \\
P_{rel} &= P_0 \left(1 - \exp^{(t_0 - t)/\tau_{rel}} \right)
\end{aligned}
\tag{2}
$$

Another significant source of depolarisation in the dendritic spine is provided by backpropagating action potentials (bAPs) from the soma (Stuart and Sakmann 1994; Magee and Johnston 1997; Palmer and Stuart 2009). In accordance with previous modelling studies, a post-synaptic action potential at time t_0 generates peak depolarisation $V_{bAP,max}$ in the spine that subsequently undergoes decay with a large, rapid component and smaller, slower component (with time constants $\tau_{bAP,f}$=3 ms and $\tau_{bAP,s}$ varying between 25 ms and 85 ms respectively), the relative contribution of each term dictated by the dimensionless positive constants $I_{bAP,f}$=0.75 and $I_{bAP,s}$=0.25 according to Eq. (3) (Shouval et al. 2002; Rackham et al. 2010).

$$
bAP(t) = V_{bAP,\max} \left(I_{bAP,f} \exp^{\left(t_0 - t/\tau_{bAP,f}\right)} + I_{bAP,s} \exp^{\left(t_0 - t/\tau_{bAP,s}\right)} \right) \tag{3}
$$

The local calcium concentration $[Ca^{2+}]$ in each dendritic spine (μM) is determined by influx through NMDAr and passive decay with a time constant τ_{Ca} according to Eq. (4); where $\overline{g}_{NMDA,Ca}$ represents the maximum calcium conductance of NMDAr, E_{Ca} the reversal potential for calcium, and the positive constant α converts ionic current to concentration change per unit time (Graupner and Brunel 2007; Rackham et al. 2010; Sabatini et al. 2002).

$$
\begin{aligned}
Ca_{NMDA} &= -\alpha \overline{g}_{NMDA,Ca} P_{NMDA} G_{NMDA} (V_N - E_{Ca}) \\
\frac{d[Ca^{2+}]}{dt} &= Ca_{NMDA} - \frac{[Ca^{2+}]}{\tau_{Ca}}
\end{aligned}
\tag{4}
$$

All relevant parameters in the neuron model are fitted to recent data from electrophysiological and fluorescent imaging studies of dendritic spines on CA1 pyramidal neurons during synaptic activation and action potential generation (Rackham et al. 2010). Maximum excitatory conductance values are chosen to match experimental recordings which indicate that an AMPAr mediated depolarisation of ~10 mV is generated in the spine by activation of a single synapse (giving $\overline{g}_{AMPA} = 23.5\text{pS}$); an NMDAr mediated depolarisation of ~5 mV is generated in the spine by activation of a single synapse in the absence of extracellular Mg^{2+} (giving $\overline{g}_{NMDA} = 3.35\text{pS}$); and bAPs generate a maximum depolarisation of $V_{bAP,max}$=67 mV in the spine unless stated otherwise (Canepari et al. 2007; Palmer and Stuart 2009; Fernandez de Sevilla et al. 2007). Maximum calcium conductance of the NMDA receptor is initially set at $\overline{g}_{NMDA,\,Ca} = 0.159\text{pS}$ to generate a peak calcium concentration of 0.17 μM from a single synaptic input at resting membrane potential, and adjusted when the temporal profile of NMDAr activation is manipulated in other simulations to provide the same peak calcium concentration (Graupner and Brunel 2007). The decay of $[Ca^{2+}]$ proceeds with a time constant of τ_{Ca}=15 ms, in line with empirical recordings of calcium dynamics in individual dendritic spines on CA1 pyramidal neurons (Sabatini et al. 2002). The source and value of all simulation parameters are given in Table 1.

4.2 Plasticity model

The majority of previous models based on the calcium control hypothesis have used an arbitrarily defined function to translate peak or integrated NMDAr-[Ca2+] values directly into synaptic weight change (Shouval et al. 2002; Rackham et al. 2010). In contrast, we make use of two intermediate dynamic pathways with distinct kinetics that independently control the probability p_x of stochastic potentiating and depressing transitions (x ∈ P,D) between binary high and low synaptic weight states w_x in a Markov model. We putatively associate the probability of low→high and high→low weight transitions with kinase and phosphatase activity respectively.

$$
\begin{aligned}
&\frac{dp_x}{dt} = -\frac{(p_x - p_{x0})}{\tau_x} \quad x \in (P, D) \\
&\sigma_x = \frac{H\left([Ca^{2+}] - \beta_x\right)\left([Ca^{2+}] - \beta_x\right)^{HN_x}}{HC_x + H([Ca^{2+}] - \beta_x)([Ca^{2+}] - \beta_x)^{HN_x}} \\
&\left.\begin{aligned}
\frac{dp_P}{dt} &= \frac{dp_P}{dt} + k_P \sigma_P \\
\frac{dp_D}{dt} &= \frac{dp_D}{dt} + k_D \sigma_D - k_I \sigma_P
\end{aligned}\right\} if \; \frac{d[Ca^{2+}]}{dt} = 0 \cap \frac{d^2[Ca^{2+}]}{dt^2} < 0 \\
&\Delta w = \frac{\sum f_P N w_P + f_D N w_D}{\sum f_{P0} N w_P + f_{D0} N w_D}
\end{aligned}
\tag{5}
$$

Transition probabilities take non-zero values p_{x0} at rest and decay with individual time constants τ_x after being perturbed by NMDAr-$[Ca^{2+}]$ dynamics that are identical across each of N=10000 simulated dendritic spines. Transition probabilities are incremented either at each time step by integrated calcium influx; or solely at local peaks in calcium concentration. In both cases, the scale of increase is calculated as the product of a positive constant k_x and modified Hill function σ_x=f($[Ca^{2+}]$) inspired by recent advances in systems biology, where H represents the Heaviside step function (Morgan 2007; Buchler and Cross 2009). These

Table 1 Parameter definitions and values used throughout the simulations presented

Notation	Parameter	Value	Source
C_m	Specific membrane capacitance	1 μF/cm^2	(Destexhe et al. 1994)
g_L	Leak conductance	0.1pS	(Destexhe et al. 1994)
A_{spine}	Spine surface area	1.75×10^{-7} cm^2	-
$\overline{g}_{AMPA}$	Peak AMPA conductance	23.5pS	Set to produce 10 mV depolarisation in the spine under total NMDAr blockade (Palmer and Stuart 2009)
$\overline{g}_{NMDA}$	Peak NMDA conductance	3.35pS	Set to produce 1 mV depolarisation in the spine under total AMPAr blockade with [Mg^{2+}]=0 mM (Johnston et al. 2003)
τ_{AMPA}	AMPA time constant	5.26 ms	(Destexhe et al. 1994)
$\tau_{NMDA,\ f}$	Fast NMDA time constant	1.485 ms	(Destexhe et al. 1994)
$\tau_{NMDA,\ s}$	Slow NMDA time constant	50 ms : 152 ms	(Destexhe et al. 1994)
E_L	Leak reversal potential	−65 mV	(Destexhe et al. 1994)
E_{AMPA}	AMPA reversal potential	0 mV	(Rubin et al. 2005; Urakubo et al. 2008; Destexhe et al. 1994)
E_{NMDA}	NMDA reversal potential	0 mV	(Rubin et al. 2005; Urakubo et al. 2008; Destexhe et al. 1994)
[Mg^{2+}]	Extracellular Magnesium concentration	1 mM	(Shouval et al. 2002; Rubin et al. 2005; Urakubo et al. 2008; Destexhe et al. 1994)
P_0	Baseline probability of release	0.5	(Shouval et al. 2002; Urakubo et al. 2008)
τ_{rel}	Time constant of short-term depression	50 ms	-
$I_{bAP,f}$	Contribution of fast bAP time constant	0.75	(Shouval et al. 2002; Urakubo et al. 2008)
$I_{bAP,s}$	Contribution of slow bAP time constant	0.25	(Shouval et al. 2002; Urakubo et al. 2008)
$\tau_{bAP,f}$	Fast bAP time constant	3 ms	(Shouval et al. 2002; Urakubo et al. 2008)
$\tau_{bAP,s}$	Slow bAP time constant	25 ms : 85 ms	(Shouval et al. 2002; Urakubo et al. 2008)
α	Constant to convert NMDA current to calcium flux	1 μM/mC	(Shouval et al. 2002; Rubin et al. 2005; Urakubo et al. 2008)
$\overline{g}_{NMDA,\ Ca}$	NMDAr calcium conductance	0.159pS	Set to produce a peak of NMDAr-[Ca^{2+}]=0.17 μM from a single pre-synaptic input (Rubin et al. 2005)
E_{Ca}	Calcium reversal potential	120 mV	(Shouval et al. 2002; Rubin et al. 2005; Urakubo et al. 2008)
τ_{Ca}	Time constant of calcium decay	15 ms	(Larkum et al. 2001)
P_{P0}	Kinase activity / transition probability at rest	3.22×10^{-6}	-
P_{D0}	Phosphatase activity / transition probability at rest	7.89×10^{-6}	-
τ_P	Kinase time constant	50 ms	-
τ_D	Phosphatase time constant	2000 ms	-
k_P	Kinase activation constant	$0.04\ /1\times10^{-3}$	-
k_D	Phosphatase activation constant	$4\times10^{-4}/4\times10^{-6}$	-
k_I	Competition constant	0.2	-
HC_P	Kinase dissociation constant	2 μM	-
HC_D	Phosphatase dissociation constant	2 μM	-
HN_P	Hill number of kinase activation	4	(Sjöström et al. 2008; Karmarkar and Buonomano 2002; Graupner and Brunel 2007)
HN_D	Hill number of phosphatase activation	3	(Sjöström et al. 2008; Karmarkar and Buonomano 2002; Graupner and Brunel 2007)
β_P	Hill threshold for kinase activation	0.175 : 0.51	-
β_D	Hill threshold for phosphatase activation	0 : 0.31	-
N	Total number of synaptic inputs	10,000	-
f_{P0}	Initial frequency of synapses in high weight state	0.29	(O'Connor et al. 2005a)
f_{D0}	Initial frequency of synapses in low weight state	0.71	(O'Connor et al. 2005a)
w_P	Putative strength of high weight state	2	(O'Connor et al. 2005a; Abarbanel et al. 2003)
w_D	Putative strength of low weight state	0.66	(O'Connor et al. 2005a; Abarbanel et al. 2003)

Hill functions incorporate an effective threshold for activation β_x below which kinase and phosphatase activity is effectively buffered and above which activation follows standard formalism (Eq. (5)). Hill coefficients HN_x and

dissociation constants HC_x are set in accordance with previous modelling studies (Zhabotinsky 2000; Abarbanel et al. 2003; Pi and Lisman 2008). The results presented here are robust to significant changes in these parameter values provided that $HN_P > HN_D$, negating the need for extensive parameter fitting (data not shown) (Zhabotinsky 2000; Abarbanel et al. 2003). The empirically observed competition between kinase and phosphatase activation is incorporated by subtracting the product of a positive constant k_I and Hill function σ_P that controls kinase activity from phosphatase activity during step changes in transition probabilities.

The initial frequency of synapses occupying high and low weight states is matched to empirical recordings in the naïve slice, with $f_{D0}=71$ % of synapses occupying the low weight state, $f_{P0}=29$ % occupying the high weight state, and the ratio of non-zero transition probabilities is set to maintain this relative frequency at rest (O'Connor et al. 2005a). In line with empirical measurements regarding the relative conductance of potentiated and depressed CA3-CA1 synapses, we set the relative strength of high and low weight states as $w_P=2$ and $w_D=0.66$ respectively (O'Connor et al. 2005a; Abarbanel et al. 2005). The overall change in synaptic weight Δw generated by various stimulation protocols can then be assessed by comparing the frequency of synaptic inputs occupying high and low weight states (f_P and f_D respectively) at the start and end of each simulation according to Eq. (5).

4.3 Simulation details

During spike pairing stimulation protocols, values of Δt describe the temporal offset between the peak of a single input EPSP and that of a single bAP; while in triplet pairing protocols, values of Δt describe the temporal offset between the peak of a single input EPSP and the second of two bAPs that are separated by a constant offset of 10 ms (Wittenberg and Wang 2006). Stimulation frequency in each case is measured as the inverse of temporal offset between the peak of successive input EPSPs. Tetanic stimulation consists of three trains of one hundred pre-synaptic inputs delivered at various frequencies, with a period of 5 min between each train (O'Connor et al. 2005b). In tetanic stimulation protocols with stochastic post-synaptic activity, periodic pre-synaptic EPSPs are followed with a probability of 22.2 % (corresponding to the ratio of two hundred post-synaptic action potentials to nine hundred volleys of pre-synaptic field stimulation observed in (Wittenberg and Wang 2006)) by a single bAP with temporal offset drawn from a random distribution with $\mu=6.2$ ms and $\sigma=4$ ms. The post-synaptic depolarisation protocol consists of delivering one hundred pre-synaptic inputs at a frequency of 2 Hz while the membrane voltage of the dendritic spine is clamped at a constant value (Ngezahayo et al. 2000). The burst frequency stimulation protocol consists of delivering forty bursts of five pre- and five post- synaptic spikes at a rate of 0.5 Hz, with equal inter-spike intervals determined by the intra-burst frequency and either the pre- or post- synaptic spike train leading the other by 6 ms (Sjöström et al. 2001; Froemke et al. 2006). The burst pairing stimulation protocol consists of ten pairings of either a single spike or burst of three spikes with an inter-spike interval of 5 ms pre- and / or post-synaptically, with the pre-synaptic activity preceding post-synaptic activity by 10 ms in all cases, at a constant frequency of 5 Hz (Pike et al. 1999). The spike triplet pairing protocol consisted of sixty pairings of one or two pre- and / or- post synaptic spikes with varying temporal offset at a constant frequency of 1 Hz or 5 Hz (Froemke et al. 2006; Wang et al. 2005). All dynamic values are calculated at each 0.1 ms timestep using Euler integration, and all simulations are performed using MATLAB.

Acknowledgments The authors would like to thank Samuel Wang, Gayle Wittenberg and Guoqiang Bi for providing experimental data.

References

Abarbanel, H. D. I., Gibb, L., Huerta, R., & Rabinovich, M. I. (2003). Biophysical model of synaptic plasticity dynamics. *Biological Cybernetics, 89*, 214–226.

Abarbanel, H. D. I., Talathi, S. S., Gibb, L., & Rabinovich, M. I. (2005). Synaptic plasticity with discrete state synapses. *Physical Review E, 72*, 031914.

Aihara, T., Abiru, Y., Yamazaki, Y., Watanabe, H., Fukushima, Y., & Tsukuda, M. (2007). The relation between spike-timing dependent plasticity and Ca^{2+} dynamics in the hippocampal CA1 network. *Neuroscience, 145*, 80–87.

Artola, A., & Singer, W. (1993). Long-term depression of excitatory synaptic transmission and its relationship to long-term potentiation. *Trends in Neuroscience, 16*, 480–487.

Bagal, A. A., Kao, J., Tang, C.-M., & Thompson, S. M. (2005). Long-term potentiation of exogenous glutamate responses at single dendritic spines. *PNAS, 102*, 14434–14439.

Bender, V. A., Bender, K. J., Brasier, D. J., & Feldman, D. E. (2006). Two coincidence detectors for spike timing-dependent plasticity in somatosensory cortex. *Journal of Neuroscience, 26*, 4166–4177.

Bi, G.-Q., & Poo, M.-M. (1998). Synaptic modifications in cultured hippocampal neurons: dependence on spike timing, synaptic strength, and postsynaptic cell type. *Journal of Neuroscience, 77*, 551–555.

Bienenstock, E. L., Cooper, L. N., & Munro, P. W. (1982). Theory for the development of neuron selectivity: orientation specificity and binocular interaction in visual cortex. *Journal of Neuroscience, 2*, 32–48.

Bliss, T., Collingridge, G., & Morris, R. (2007). Synaptic plasticity in the hippocampus. In P. Andersen, R. Morris, D. Amaral, T. Bliss, J. O'Keefe (Eds.), *The hippocampus book* (pp. 343–474). Oxford University Press.

Buchanan, K. A., & Mellor, J. R. (2007). The development of synaptic plasticity induction rules and the requirement for postsynaptic spikes in rat hippocampal CA1 pyramidal neurones. *The Journal of Physiology, 585*, 429–445.

Buchanan, K. A., & Mellor, J. R. (2010). The activity requirements for spike timing-dependent plasticity in the hippocampus. *Frontiers in Synaptic Neuroscience, 2*, 11.

Buchler, N. E., & Cross, F. R. (2009). Protein sequestration generates a flexible ultrasensitive response in a genetic network. *Molecular Systems Biology, 5*, 272.

Buonomano, D. V. (2005). A learning rule for the emergence of stable dynamics and timing in recurrent networks. *Journal of Neurophysiology, 94*, 2275–2283.

Bush, D., Philippides, A., Husbands, P., & O'Shea, M. (2010). Dual coding with STDP in an auto-associative network model of the hippocampus. *PLoS Computational Biology, 6*, e1000839.

Buzsáki, G. (2010). Neural syntax: cell assemblies, synapsembles, and readers. *Neuron, 68*, 362–385.

Canepari, M., Djurisic, M., & Zecevic, D. (2007). Dendritic signals from rat hippocampal CA1 pyramidal neurons during coincident pre- and post- synaptic activity: a combined voltage- and calcium-imaging study. *The Journal of Physiology, 580*, 463–484.

Caporale, N., & Dan, Y. (2008). Spike timing-dependent plasticity: a Hebbian learning rule. *Annual Reviews in Neuroscience, 31*, 25–46.

Christie, B. R., Magee, J. C., & Johnston, D. (1996). The role of dendritic action potentials and Ca^{2+} influx in the induction of homosynaptic long-term depression in hippocampal CA1 pyramidal neurons. *Learning and Memory, 3*, 160–169.

Citri, A., & Malenka, R. C. (2008). Synaptic plasticity: multiple forms, functions, and mechanisms. *Neuropsychopharmacology, 33*, 18–41.

Cooke, S. F., & Bliss, T. V. P. (2006). Plasticity in the human central nervous system. *Brain, 129*, 1659–1673.

Cormier, R. J., Greenwood, A. C., & Connor, J. A. (2001). Bidirectional synaptic plasticity correlated with the magnitude of dendritic calcium transients above a threshold. *Journal of Neurophysiology, 85*, 399–406.

Dayan, P., & Abbott, L. F. (2001). *Theoretical neuroscience* (pp. 180–183). London: MIT.

Debanne, D., Gähwiler, B. H., & Thompson, S. M. (1998). Long-term synaptic plasticity between pairs of individual CA3 pyramidal cells in rat hippocampal slice cultures. *The Journal of Physiology, 507*, 237–247.

Desai, N. S. (2003). Homeostatic plasticity in the CNS: synaptic and intrinsic forms. *Journal of Physiology, Paris, 97*, 391–402.

Destexhe, A., Mainen, Z., & Sejnowski, T. (1994). Synthesis of models for excitable membranes, synaptic transmission and neuromodulation using a common kinetic formalism. *Journal of Computational Neuroscience, 1*, 195–230.

Dudek, S. M., & Bear, M. F. (1992). Homosynaptic long-term depression in area CA1 of hippocampus and effects of N-methyl-D-aspartate receptor blockade. *PNAS, 89*, 4363–4367.

Dudman, J. T., Tsay, D., & Siegelbaum, S. A. (2007). A role for synaptic inputs at distal dendrites: instructive signals for hippocampal long-term plasticity. *Neuron, 56*, 866–879.

Erreger, K., Dravid, S. M., Banke, T. G., Wyllie, D. J. A., & Traynelis, S. F. (2005). Subunit-specific gating controls rat NR1/NR2A and NR1/NR2B NMDA channel kinetics and synaptic signalling profiles. *The Journal of Physiology, 563*, 345–358.

Fan, Y., Fricker, D., Brager, D. H., Chen, X., Lu, H.-C., Chitwood, R. A., & Johnston, D. (2005). Activity-dependent decrease of excitability in rat hippocampal neurons through increases in I_h. *Nature Neuroscience, 8*, 1542–1551.

Fernandez de Sevilla, D., Fuenzalida, M., Porto Pazos, A. B., & Buno, W. (2007). Selective shunting of the NMDA EPSP component by the slow afterhyperpolarisation in rat CA1 pyramidal neurons. *Journal of Neurophysiology, 97*, 3242–3255.

Fiete, I. R., Senn, W., Wang, C., & Hahnloser, R. H. R. (2010). Spike time-dependent plasticity and heterosynaptic competition organize networks to produce long scale-free sequences of neural activity. *Neuron, 65*, 563–576.

Frey, U., & Morris, R. G. (1997). Synaptic tagging and long-term potentiation. *Nature, 385*, 533–536.

Frick, A., Magee, J., & Johnston, D. (2004). LTP is accompanied by an enhanced local excitability of pyramidal neuron dendrites. *Nature Neuroscience, 7*, 126–135.

Froemke, R. C., Poo, M. M., & Dan, Y. (2005). Spike-timing-dependent synaptic plasticity depends on dendritic location. *Nature, 434*, 221–225.

Froemke, R. C., Tsay, I. H., Raad, M., Long, J. D., & Dan, Y. (2006). Contribution of individual spikes in burst-induced long-term synaptic modification. *Journal of Neurophysiology, 95*, 1620–1629.

Froemke, R. C., Debanne, D., & Bi, G. Q. (2010). Temporal modulation of spike-timing-dependent plasticity. *Frontiers in Synaptic Neuroscience, 2*, 19.

Fukunaga, K., Muller, D., Ohmitsu, M., Bako, E., DePaoli-Roach, A. A., & Miyamoto, E. (2000). Decreased protein phosphatase 2A activity in hippocampal long-term potentiation. *Journal of Neurochemistry, 74*, 807–817.

Gerkin, R. C., Lau, P.-M., Nauen, D. W., Wang, Y. T., & Bi, G.-Q. (2007). Modular competition driven by NMDA receptor subtypes in spike-timing-dependent plasticity. *Journal of Neurophysiology, 97*, 2851–2862.

Graupner, M., & Brunel, N. (2007). STDP in a bistable synapse model based on CaMKII and associated signalling pathways. *PLoS Computational Biology, 3*(11), e221.

Graupner, M., & Brunel, N. (2010). Mechanisms of induction and maintenance of spike-timing dependent plasticity in biophysical synapse models. *Frontiers in Computational Neuroscience, 4*, 136.

Hanson, P. I., & Schulman, H. (1992). Neuronal Ca2+ / Calmodulin-dependent protein kinase. *Annual Review of Biochemistry, 61*, 559–601.

Harris, K. M., & Kater, S. B. (1994). Dendritic spines: cellular specialisations imparting both stability and flexibility to synaptic function. *Annual Reviews in Neuroscience, 17*, 341–371.

Harris, K. D., Hirase, H., Leinekugel, X., Henze, D. A., & Buzsaki, G. (2001). Temporal interaction between single spikes and complex spike bursts in hippocampal pyramidal cells. *Neuron, 32*, 141–149.

Hebb, D. O. (1949). *The organisation of behaviour*. New York: Wiley.

Jahr, C. E., & Stevens, C. F. (1990). A quantitative description of NMDA receptor-channel kinetic behaviour. *Journal of Neuroscience, 10*, 1830–1837.

Johnston, D., Christie, B. R., Frick, A., Gray, R., Hoffman, D. A., Schexnayder, L. K., Watanabe, S., & Yuan, L.-L. (2003). Active dendrites, potassium channels and synaptic plasticity. *Philosophical Transactions of the Royal Society B, 358*, 667–674.

Kampa, B. M., Letzkus, J. J., & Stuart, G. J. (2007). Dendritic mechanisms controlling spike-timing dependent plasticity. *Trends in Neuroscience, 30*, 456–463.

Karmarkar, U. R., & Buonomano, D. V. (2002). A model of spike-timing dependent plasticity: one or two coincidence detectors? *Journal of Neurophysiology, 88*, 507–513.

Krug, M., Lossner, B., & Ott, T. (1984). Anisomycin blocks the late phase of long-term potentiation in the dentate gyrus of freely moving rats. *Brain Research Bulletins, 13*, 39–42.

Larkum, M. E., Zhu, J. J., & Sakmann, B. (2001). Dendritic mechanisms underlying the coupling of the dendritic with the axonal action potential initiation zone of adult rat layer 5 pyramidal neurons. *The Journal of Physiology, 533*, 447–466.

Larson, J., Wong, D., & Lynch, G. (1986). Patterned stimulation at the theta frequency is optimal for the induction of hippocampal long-term potentiation. *Brain Research, 368*, 347–350.

Lazar, A., Pipa, G., & Triesch, J. (2009). SORN: a self-organizing recurrent neural network. *Frontiers in Computational Neuroscience, 3*, 23.

Lee, H.-K., Barbarosie, M., Kameyama, K., Bear, M. F., & Huganir, R. L. (2000). Regulation of distinct AMPA receptor phosphorylation sites during bidirectional synaptic plasticity. *Nature, 405*, 955–959.

Legenstein, R., & Maass, W. (2011). Branch-specific plasticity enables self-organisation of nonlinear computation in single neurons. *Journal of Neuroscience, 31*, 10787–10802.

Lisman, J. (1989). A mechanism for the Hebb and the anti-Hebb processes underlying learning and memory. *PNAS, 86*, 9574–9578.

Lisman, J. E. (1997). Bursts as a unit of neural information: making unreliable synapses reliable. *Trends in Neurosciences, 20*, 38–43.

Lisman, J., & Spruston, N. (2005). Postsynaptic depolarisation requirements for LTP and LTD: a critique of spike-timing dependent plasticity. *Nature Neuroscience, 8*, 839–841.

Lomo, T., & Bliss, T. V. (1973). Long-lasting potentiation of synaptic transmission in the dentate area of the anaesthetized rabbit following stimulation of the perforant path. *The Journal of Physiology, 232*, 331–356.

Losonczy, A., Makara, J. K., & Magee, J. C. (2008). Compartmentalised dendritic plasticity and input feature storage in neurons. *Nature, 452*, 436–441.

Magee, J. C., & Johnston, D. (1997). A synaptically controlled, associative signal for Hebbian plasticity in hippocampal neurons. *Science, 275*, 209–213.

Malenka, R. C., & Bear, M. F. (2004). LTP and LTD: an embarrassment of riches. *Neuron, 44*, 5–21.

Malenka, R. C., & Nicoll, R. A. (1999). Long-term potentiation—a decade of progress? *Science, 285*, 1870–1874.

Malenka, R. C., Kauer, J. A., Perkel, D. J., Mauk, M. D., Kelly, P. T., Nicoll, R. A., & Waxham, M. N. (1989). An essential role for postsynaptic calmodulin and protein kinase activity in long-term potentiation. *Nature, 340*, 554–557.

Malinow, R., Schulman, H., & Tsien, R. W. (1989). Inhibition of postsynaptic PKC or CaMKII blocks induction but not expression of LTP. *Science, 245*, 862–866.

Martin, S. J., Grimwood, P. D., & Morris, R. G. M. (2000). Synaptic plasticity and memory: an evaluation of the hypothesis. *Annual Review of Neuroscience, 23*, 649–711.

Meredith, R. M., Floyer-Lea, A. M., & Paulsen, O. (2003). Maturation of long-term potentiation induction rules in rodent hippocampus: role of GABAergic inhibition. *Journal of Neuroscience, 23*, 11142–11146.

Mizuno, T., Kanazawa, I., & Sakurai, M. (2001). Differential induction of LTP and LTD is not determined solely by instantaneous calcium concentration: an essential involvement of a temporal factor. *European Journal of Neuroscience, 14*, 701–708.

Morgan, D. O. (2007). *The cell cycle: Principles of control*. Sunderland: New Science Press.

Mulkey, R. M., Herron, C. E., & Malenka, R. C. (1993). An essential role for protein phosphatases in hippocampal long-term depression. *Science, 261*, 1104–1107.

Nelson, S. B., & Turrigiano, G. G. (2008). Strength through diversity. *Neuron, 60*, 477–482.

Neves, G., Cooke, S. F., & Bliss, T. V. P. (2008). Synaptic plasticity, memory and the hippocampus: a neural network approach to causality. *Nature Reviews Neuroscience, 9*, 65–75.

Nevian, T., & Sakmann, B. (2006). Spine Ca2+ signaling in spike-timing-dependent plasticity. *Journal of Neuroscience, 26*, 11001–11013.

Ngezahayo, A., Schachner, M., & Artola, A. (2000). Synaptic activity modulates the induction of bidirectional synaptic changes in adult mouse hippocampus. *Journal of Neuroscience, 20*, 2451–2458.

Nguyen, P. V., Abel, T., & Kandel, E. R. (1994). Requirement of a critical period of transcription for induction of a late phase of LTP. *Science, 165*, 1104–1107.

Nishiyama, M., Hong, K., Mikoshiba, K., Poo, M. M., & Kato, K. (2000). Calcium stores regulate the polarity and input specificity of synaptic modification. *Nature, 408*, 584–588.

O'Connor, D. H., Wittenberg, G. M., & Wang, S. S. H. (2005a). Graded bidirectional synaptic plasticity is composed of switch-like unitary events. *PNAS, 102*, 9679–9684.

O'Connor, D. H., Wittenberg, G. M., & Wang, S. S. H. (2005b). Dissection of bidirectional synaptic plasticity into saturable unidirectional processes. *Journal of Neurophysiology, 94*, 1565–1573.

Palmer, L. M., & Stuart, G. J. (2009). Membrane potential changes in dendritic spines during action potentials and synaptic input. *Journal of Neuroscience, 29*, 6897–6903.

Perez-Otano, I., & Ehlers, M. D. (2005). Homeostatic plasticity and NMDA receptor trafficking. *Trends in Neurosciences, 28*, 229–238.

Petersen, C. C. N., Malenka, R. C., Nicoll, R. A., & Hopfield, J. J. (1998). All-or-none potentiation at CA3-CA1 synapses. *PNAS, 95*, 4732–4737.

Pfister, J.-P., & Gerstner, W. (2006). Triplets of spikes in a model of spike timing-dependent plasticity. *Journal of Neuroscience, 26*, 9673–9682.

Pi, H. J., & Lisman, J. E. (2008). Coupled phosphatase and kinase switches produce the tristability required for long-term potentiation and long-term depression. *Journal of Neuroscience, 28*, 13132–13138.

Pike, F. G., Meredith, R. M., Olding, A. W., & Paulsen, O. (1999). Postsynaptic bursting is essential for 'Hebbian' induction of associative long-term potentiation at excitatory synapses in rat hippocampus. *The Journal of Physiology, 518*, 571–576.

Rackham, O. J. L., Tsaneva-Atanasova, K., Ganesh, A., & Mellor, J. R. (2010). A Ca^{2+}-based computational model for NMDA receptor-dependent synaptic plasticity at individual post-synaptic spines in the hippocampus. *Frontiers in Synaptic Neuroscience, 2*, 31.

Rodríguez-Moreno, A., & Paulsen, O. (2008). Spike timing-dependent long-term depression requires presynaptic NMDA receptors. *Nature Neuroscience, 11*, 744–745.

Rubin, J. E., Gerkin, R. C., Bi, G.-Q., & Chow, C. C. (2005). Calcium time course as a signal for spike-timing-dependent plasticity. *Journal of Neurophysiology, 93*, 2600–2613.

Sabatini, B. L., Oertner, T. G., & Svoboda, K. (2002). The life cycle of Ca^{2+} ions in dendritic spines. *Neuron, 33*, 439–452.

Shouval, H. Z., & Kalantzis, G. (2005). Stochastic properties of synaptic transmission affect the shape of spike time-dependent plasticity curves. *Journal of Neurophysiology, 93*, 1069–1073.

Shouval, H. Z., Bear, M. F., & Cooper, L. N. (2002). A unified model of NMDA receptor-dependent bidirectional synaptic plasticity. *PNAS, 99*, 10831–11083.

Shouval, H. Z., Wang, S. S.-H., & Wittenberg, G. M. (2010). Spike timing dependent plasticity: a consequence of more fundamental learning rules. *Frontiers in Computational Neuroscience, 4*, 19.

Sjostrom, P. J., & Nelson, S. B. (2002). Spike timing, calcium signals and synaptic plasticity. *Current Opinion in Neurobiology, 12*, 305–314.

Sjöström, P. J., Turrigiano, G. G., & Nelson, S. B. (2001). Rate, timing, and cooperativity jointly determine cortical synaptic plasticity. *Neuron, 32*, 1149–1164.

Sjöström, P. J., Turrigiano, G. G., & Nelson, S. B. (2003). Neocortical LTD via coincident activation of presynaptic NMDA and cannabinoid receptors. *Neuron, 39*, 641–654.

Sjöström, P. J., Rancz, E. A., Roth, A., & Häusser, M. (2008). Dendritic excitability and synaptic plasticity. *Physiological Reviews, 88*, 769–840.

Song, S., Miller, K. D., & Abbott, L. F. (2000). Competitive Hebbian learning through spike-timing dependent synaptic plasticity. *Nature Neuroscience, 3*, 919–926.

Stuart, G. J., & Sakmann, B. (1994). Active propagation of somatic action potentials into neocortical pyramidal cell dendrites. *Nature, 367*, 69–72.

Urakubo, H., Honda, M., Froemke, R. C., & Kuroda, S. (2008). Requirement of an allosteric kinetics of NMDA receptors for spike-timing dependent plasticity. *Journal of Neuroscience, 28*, 3310–3323.

Wang, H. X., Gerkin, R. C., Nauen, D. W., & Bi, G.-Q. (2005). Coactivation and timing-dependent integration of synaptic potentiation and depression. *Nature Neuroscience, 8*, 187–193.

Watt, A. J., Sjostrom, P. J., Hausser, M., Nelson, S. B., & Turrigiano, G. G. (2004). A proportional but slower NMDA potentiation follows AMPA potentiation in LTP. *Nature Neuroscience, 7*, 518–524.

Whitlock, J. R., Heynen, A. J., Shuler, M. G., & Bear, M. F. (2006). Learning induces long-term potentiation in the hippocampus. *Science, 313*, 1093–1097.

Wittenberg, G. M., & Wang, S.-S. H. (2006). Malleability of spike-timing-dependent plasticity at the CA3-CA1 synapse. *Journal of Neuroscience, 26*, 6610–6617.

Yang, S. N., Tang, Y. G., & Zucker, R. (1999). Selective induction of LTP and LTD by post-synaptic $[Ca^{2+}]_i$ elevation. *Journal of Neurophysiology, 81*, 781–787.

Zhabotinsky, A. M. (2000). Bistability in the Ca2+ / calmodulin-dependent protein kinase-phosphatase system. *Biophysical Journal, 79*, 2211–2221.